To avoid issues relating to nomenclatural acts, minor sections of this article which reported on the naming of a new species, and which did not make it into the final publication, have been redacted.

[redacted] [redacted] a new fossil inioid (Mammalia: Cetacea) from the Chagres Formation of Panama and the evolution of "river dolphins" in the Americas

Nicholas D Pyenson, Jorge Velez-Juarbe, Carolina S. Gutstein, Holly Little, Dioselina I Vigil, Aaron O'Dea

In contrast to dominant mode of ecological transition in the evolution of marine mammals, different lineages of toothed whales (Odontoceti) have repeatedly invaded freshwater ecosystems during the Cenozoic era. The so-called “river dolphins” are now recognized as independent lineages that converged on similar morphological specializations (e.g., longirostry). In South America, the two endemic “river dolphin” lineages form a clade (Inioidea), with closely related fossil inioids from marine rock units in the South Pacific and North Atlantic Oceans. Here we describe a new species of fossil inioid, [redacted] nov. gen., nov. sp., from the late Miocene of Panama. The type and only known specimen consists of a partial skull, mandibles, isolated teeth, and a right scapula recovered from the Piña facies of the Chagres Formation, along the Caribbean coast of Panama. Sedimentological and associated fauna from the Piña facies point to fully marine conditions with high planktonic productivity 6.8-7.5 million years ago (middle Messinian to earliest Tortonian), which predates final closure of the Isthmus of Panama. Along with ecomorphological data, we propose that [redacted] was primarily a marine inhabitant, similar to modern oceanic delphinoids. Phylogenetic analysis of fossil and living inioids, including new codings for *Ischyrorhynchus*, a poorly described taxon from the late Miocene of Argentina, places [redacted] as the sister taxon to *Inia*, in a broader clade (Pan-Iniidae) that includes *Ischyrorhynchus* and *Meherrinia*. This phylogenetic hypothesis complicates the possible scenarios for the freshwater invasion of the Amazon River system by pan-iniids, but it remains consistent with their broader marine ancestry. Based on the fossil record of this group, along with [redacted] we propose that the ancestor of *Inia* invaded the Brazil Craton during eustatic sea-level highs during the late Miocene.

PeerJ

[redacted] a new fossil inioid (Mammalia: Cetacea) from the Chagres Formation of Panama and the evolution of "river dolphins" in the Americas

Nicholas D. Pyenson*[1,2], Jorge Vélez-Juarbe[3], Carolina S. Gutstein[1,4], Holly Little[1], Dioselina Vigil[5], and Aaron O'Dea[5]

[1]Department of Paleobiology, National Museum of Natural History, Smithsonian Institution, PO Box 37012, Washington, DC 20013, USA

[2]Departments of Mammalogy and Paleontology, Burke Museum of Natural History and Culture, Seattle, WA 98195, USA

[3]Department of Mammalogy, Natural History Museum of Los Angeles County, Los Angeles, CA 90007, U.S.A.

[4]Red Paleontológica, Laboratorio de Ontogenia y Filogenia, Departamento de Biología, Facultad de Ciencias, Universidad de Chile, Las Palmeras, Santiago 3425, Chile

[5]Smithsonian Tropical Research Institute, PO Box 0843-03092, Balboa, Republic of Panama

*Author for correspondence. Email: pyensonn@si.edu

Abstract [282/300 words]

In contrast to dominant mode of ecological transition in the evolution of marine mammals, different lineages of toothed whales (Odontoceti) have repeatedly invaded freshwater ecosystems during the Cenozoic era. The so-called "river dolphins" are now recognized as independent lineages that converged on similar morphological specializations (e.g., longirostry). In South America, the two endemic "river dolphin" lineages form a clade (Inioidea), with closely related fossil inioids from marine rock units in the South Pacific and North Atlantic Oceans. Here we describe a new genus and species of fossil inioid, [redacted] nov. gen., nov. sp., from the late Miocene of Panama. The type and only known specimen consists of a partial skull, mandibles, isolated teeth, and a right scapula recovered from the Piña facies of the Chagres Formation, along the Caribbean coast of Panama. Sedimentological and associated fauna from the Piña facies point to fully marine conditions with high planktonic productivity 6.8-7.5 million years ago (middle Messinian to earliest Tortonian), which predates formation of the Isthmus of Panama. Along with ecomorphological data, we propose that [redacted] was primarily a marine inhabitant, similar to modern oceanic delphinoids. Phylogenetic analysis of fossil and living inioids, including new codings for *Ischyrorhynchus*, a poorly described taxon from the late Miocene of Argentina, places [redacted] as the sister taxon to *Inia*, in a broader clade (Pan-Iniidae) that includes *Ischyrorhynchus* and *Meherrinia*. This phylogenetic hypothesis complicates the possible scenarios for the freshwater invasion of the Amazon River system by pan-iniids, but it remains consistent with their broader marine ancestry. Based on the fossil record of this group, along with [redacted] we propose that the ancestor of *Inia* invaded the Brazil Craton during eustatic sea-level highs during the late Miocene.

Introduction

In the evolution of marine mammals, the dominant mode of ecological transitions (*sensu* Vermeij & Dudley, 2000) is the successful adaptation to marine life from terrestrial ancestry (Thewissen & Williams, 2002; Gingerich, 2005; Kelley & Pyenson, 2015). However, the direction of this ecological transition is not exclusively from land to sea: throughout the late Cenozoic, several lineages of cetaceans and pinnipeds have evolved exclusively freshwater habitats from a marine ancestry (Hamilton et al., 2001; Pyenson et al., 2014). Among cetaceans, the group of extant "river dolphins" are the best exemplars of this ecological mode. This non-monophyletic (i.e., paraphyletic or possibly polyphyletic) group includes four different living genera (*Platanista*, *Lipotes*, *Inia*, and *Pontoporia*) that show broad morphological similarities, including longirostral skulls and jaws, reduced orbits, flexible necks, and broad, paddle-shaped flippers (Geisler et al. 2011). Notably, this assemblage of broadly convergent taxa have a biogeographic distribution across different, large freshwater river systems of South Asia and South America, and in estuarine and coastal waters of the latter as well. The advent of molecular phylogenies clarified that these lineages are not all directly related to one another, although both molecular and morphological analyses consistently group the two South American genera, *Inia* and *Pontoporia*, as sister taxa (Inioidea *sensu* Muizon, 1988a). *Lipotes*, which was endemic to the Yangtze River of China and is likely extinct (Turvey et al., 2010), may be the sister taxon to Inioidea (see Geisler et al., 2011), but these relationships are unstable because there is poor phylogenetic resolution for the placement of *Lipotes* and *Platanista* among basal branching lineages of Odontoceti (Messenger & McGuire, 1998; Hamilton et al., 2001; Nikaido et al., 2001; Geisler & Sanders, 2003; Arnason et al., 2004; May-Collado & Agnarsson, 2006; Steeman et al., 2009; Geisler et al. 2011).

With restricted distributions, serious conservation threats, and relatively low taxonomic richness compared with other odontocete clades, the evolutionary history of "river dolphins" remains a topic of

perennial interest (Cassens et al., 2000; Hamilton et al., 2001; Nikaido et al., 2001; Pyenson, 2009; Ruiz-Garcia & Shostell, 2010; Turvey et al. 2010; Geisler et al. 2011). The fossil record of South Asian "river dolphins" is poor, with no taxa reported from undisputable remains (e.g., *Prolipotes* is known only from an isolated mandible that cannot be clearly diagnosed). By contrast, fossil South American "river dolphins" has have been reported from Neogene rocks of South America since the 1850s (Cozzuol, 1996). The majority of these fossil taxa have been assigned to either Iniidae or Pontoporiidae, based on diagnostic features of the face and vertex (Muizon, 1988a), and include taxa (e.g., *Pontistes*, *Pliopontos*, *Brachydelphis*) known from marine rocks units of middle Miocene through early Pliocene age in Argentina, Peru, and Chile (Muizon, 1984; Muizon, 1988b; Cozzuol, 1996; Gutstein et al. 2009; Lambert & Muizon, 2013; Gutstein et al. 2014a). Recently, Bianucci et al. (2013) reported an isolated periotic with diagnostic features of Platanistinae (today limited to South Asia) from the Peruvian Amazon Basin of Laventan South American Land Mammal Age. This finding is striking for its disjunct biogeographic occurrence, relative to living *Platanista* in South Asia, but it is consistent with the widespread distribution of fossil platanistoids reported elsewhere in the world from late Paleogene through Neogene rocks of the South and North Pacific and the North Atlantic oceans (Fordyce, 2009).

Similarly, the fossil record of inioids extends well beyond South America. Fossil pontoporiids have been described from shallow marine and estuarine strata of early late Miocene to early Pliocene age from the Atlantic coast of North America, including Maryland, Virginia, North Carolina and Florida (Morgan, 1994; Whitmore, 1994; Godfrey & Barnes, 2008; Gibson & Geisler, 2009; Geisler et al. 2012). Along the Atlantic coast of Europe, *Protophocaena minima*, originally described by Abel (1905) from shallow marine Miocene of the Netherlands, is now recognized as a pontoporiid (Lambert & Post, 2005) based on additional cranial and periotic material from the Miocene of Belgium and the

Netherlands. Pyenson & Hoch (2007) reported pontoporiids (cf. *Brachydelphis* and *Pontistes*) from the marine Gram Formation in Denmark, which is early late Miocene age. To date, no fossil pontoporiids have been described from the North Pacific Ocean; *Parapontoporia* spp., which are well known from abundant Mio-Pliocene localities in northern and southern California (Boessenecker & Poust, 2015), are not pontoporiids, but belong in a clade with *Lipotes vexillifer* (Geisler et al. 2012), although *Parapontoporia* is sometimes also grouped with *Platanista, Lipotes* and *Ischyrorhynchus* (Aguirre-Fernández & Fordyce, 2014). Historically, fossils referred to Iniidae include a variety of taxa (e.g., *Goniodelphis hudsoni*, *Meherrinia isoni*, *Ischyrorhynchus vanbenedeni*), supplementing the existing data showing a much broader geographic extent for inioids in the fossil record than today. These fossil occurrences thus raise the question of how Inioidea evolved, and the evolutionary scenarios that led to their current distribution.

Here we describe a new genus and new species of Inioidea, based on a relatively complete skull, mandibles, and a right scapula from the late Miocene of Panama. This specimen was initially discovered in an intertidal zone outcrop of the Chagres Formation, near the town of Piña, along the Caribbean coastline of Panama, in early 2011 (Figure 1). The infrequency of low tides at the type locality of this specimen created a narrow window of time for excavating the specimen, which several co-authors (NDP, JVJ, DV and AO) undertook on 18 June 2011 with the assistance of staff from Smithsonian Tropical Research Institute (STRI). After exporting the specimen under permits from Panama's Ministerio de Comercio e Industrias (number DNRM-MC-074-11) to the Smithsonian's National Museum of Natural History (NMNH) in Washington, D.C., U.S.A., the specimen was prepared using mechanical tools and consolidated using standard fossil vertebrate preparation techniques by D. Vigil, S. Jabo, and P. Kroehler in the Vertebrate Paleontology Preparation Laboratory in the Department of Paleobiology at NMNH.

Methods

Specimens Observed

Auroracetus bakerae (USNM 534002), *Inia geoffrensis* (USNM 395415, 49582, 239667); *Incacetus broggii* (AMNH 32656); *Ischyrorhynchus vanbenedeni* (MACN 15135, MLP 5-16), *Lipotes vexillifer* (AMNH 57333, USNM 218293), *Meherrinia isoni* (USNM 559343, identified by J. A. Geisler), *Pontoporia blainvillei* (USNM 482727, 482771, 482707).

Digital Methods

During excavation at the type locality (Figure 2), we documented *in situ* skeletal remains using a Flip camera (Cisco Systems, 2011) on time-lapse settings. Later, subsequent to the specimen's preparation in the Department of Paleobiology at USNM, we used computed tomography (CT) to scan the type specimen USNM 546125 in the Department of Anthropology with a Siemens Somatom Emotion 6 at slice thickness of 0.63 mm (which results in a three-dimensional reconstruction increment of 0.30 mm). The resultant DICOM files were processed by loading image files in Mimics (Materialise NV, Leuven, Belgium), and a mask was created based on the threshold of bone, relative to the nominal density of air. We then created a three-dimensional (3D) object from this mask, and exported the resultant file as an ASCII STL, which was opened in Geomagic (ver. 2012) for final imaging edits. We also attempted to use laser surface scanning (i.e., laser arm scanner) to capture 3D data, but line of sight issues with overhanging morphological features and the geometric complexity of the type specimen prevented a full capture of the surface geometry. As a result, we elected to use the 3D models of the skull, mandibles and scapula of USNM 546125 generated from CT data because the morphology was fully captured. After converting the CT files into 3D data, the watertight model was then processed in Autodesk Maya (ver. 2013) by Pixeldust Studios (Bethesda, Maryland), decimating the models to

100,000 triangles and creating diffuse, normal, and occlusion texture maps. The resultant 3D surface model datasets, processed from the computed tomography scans, provided sub-millimeter accuracy, and full resolution files can be downloaded at the open-access Smithsonian X 3D browser (http://3d.si.edu).

Phylogenetic Analysis

Recent work on the systematics of living and extinct odontocetes has recently provided several phylogenetic frameworks to use in this study. Geisler et al. (2011) used a combined morphological and molecular analysis to clarify the relationships among extant and fossil lineages of cetaceans, with mostly a focus on odontocetes, including some important fossil taxa, but taxon sampling within Inioidea was relatively sparse compared to Geisler et al. (2012). This latter work, which described *Meherinnia isoni*, a late Miocene inioid from marine rocks of North Carolina, U.S.A., also included other fossil inioids such as *Auroracetus bakerae*, *Ischyrorhynchus vanbenedeni*, *Protophocaena minima*, and *Stenasodelphis russellae*, some of which were not included in subsequent phylogenetic analyses of odontocetes, such as the one by Murakami et al. (2014). The starting point for our analysis was the matrix provided by Aguirre-Fernández & Fordyce (2014) in their description of the early Miocene stem odontocete *Papahu taitapu*, which used the morphological partition of Geisler et al. (2012) in their description of *Meherrinia*, along with some important modifications (e.g., the removal of Mysticeti and unpublished specimens, and coding revisions for *Waipatia* and *Prosqualodon*) that enhanced its utility for fossil odontocetes.

We added both [redacted] and *Ischyrorhynchus* as operational taxonomic units to the Aguirre-Fernández & Fordyce (2014) matrix of 311 characters, and updated the character scoring for *Ischyrorhynchus*, which was the only inioid taxon not coded from direct observation in any previous

study. The codings for *Ischyrorhynchus* herein were made by one of the authors of this study (CSG), who reviewed all the specimens in Argentina (e.g., MLP 5-16, MACN 15135), which resulted in modifications for 20 character codings (see Supplemental Information S1). The cladistic search was performed in PAUP* (Swofford, 2002) using all characters as unordered. We first performed a heuristic search using the tree bisection-reconnection (TBR) algorithm. In addition, we conducted statistical support analyses by searching for successive longer trees to calculate decay indices and 1000 bootstrap replicates. The complete matrix is available in the Supplemental Information material as see Supplemental File S1.

Results

Systematic Paleontology

Cetacea Brisson, 1762

Odontoceti Flower, 1867

Delphinida Muizon, 1988a

Inioidea Gray, 1846 *sensu* Muizon 1988a

Pan-Iniidae new clade name

[redacted] gen. nov.

Type and Only Known Species. [redacted] [redacted] sp. nov.

Etymology. *Carib*- reflects the type specimen's provenance from the shores of the Caribbean Sea, which honors the indigenous Carib tribes and follows the legacy of other fossil marine mammals described from this region, including *Caribosiren turneri* by Reinhart (1959). The feminine epithet *Inia*

reflects its similarities to the living Amazon River dolphin (*Inia geoffrensis*). Pronunciation: 'Ka-ree-bin-ee-a,' or [redacted] with the emphasis on the first vowel.

Age. Same as that of the species.

Diagnosis. Same as that of the species.

[redacted] [redacted] sp. nov. (Figs. 3-9; Tables 1-3)

Holotype. USNM 546125, consisting of an incomplete skull, both right and left mandibles, and an incomplete right scapula. The skull lacks the basicranium and tympanoperiotics. The holotype was collected by N. D. Pyenson, J. Vélez-Juarbe, A. O'Dea, D. Vigil, with assistance from staff from STRI, in 2011.

Type locality. STRI locality 650009 (9°16′55.4880″ N, 80°02′49.9200″ W), a few kilometers northeast of the town of Piña, along coastline of Panama along the Caribbean Sea (Figure 1).

Formation. Piña Facies of the Chagres Formation.

Age. Late Miocene (late Tortonian-early Messinian; ~7.5-6.8 Ma; Hendy et al., in press).

Diagnosis. [redacted] is a medium sized crown odontocete (approximately 285 cm in total length), which can be can differentiated from other cetaceans by the following combination of character states: Odontoceti based on the posterior process of premaxillae reaching beyond anterior edge of supraorbital

processes of the front (c. 74[2]); presence of maxilla overlapping frontal (c. 76[2], 77[4]); Inioidea based on the presence of a very long mandibular symphysis (c. 39[2]), a fused mandibular symphysis (c. 40[0]), a lacrimal that wraps around anterior edge of supraorbital process of frontal and slightly overlies its anterior end (c. 51[1]), and the maxilla forming the dorsolateral edge of the ventral infraorbital foramen (c. 57[1]).

[redacted] is characterized by the following unique combination of characters amongst Inioidea: rostral constriction well anterior to antorbital notch (c. 6[1]), shared with *Pontoporia*; posterior edge of rostral edge bowed forming a deep U-shaped antorbital notch (c. 11[2]), shared with *Brachydelphis* spp.; small transverse distance between lateral edges of left and right premaxillae at antorbital notch (c. 66[0]), shared with *Auroracetus* and *Inia*; short posterolateral sulcus (c. 72[1]), shared with *Protophocoena*, *Stenasodelphis* and *Auroracetus*); thickened anterolateral corner of maxilla over supraorbital process of frontal (c. 78[1]), shared with *Pontoporia* and *Stenasodelphis*; presence of a maxillary ridge (c. 79[1]), shared with *Brachydelphis mazeasi*; V-shaped anterior edge of nasal opening (c. 81[0]), shared with *Protophocoena* and *Auroracetus*; posterior end of premaxilla adjacent to lateral edge of nasal opening (c. 89[0]), shared with *Brachydelphis*; suture with left and right nasals and right and left frontals shifted towards the left (c. 114[1]), shared with *Pliopontos* and *Inia*; nasals that are anteroposteriorly elongated (c. 117[0]), shared with all inioids except *Ischyrorhynchus* and *Inia*; supraoccipital below frontal and/or nasals (c. 128[0]), shared with *Protophocoena*, *Meherrinia* and *Ischyrorhynchus*; dorsal margin of mesethmoid at same level of premaxilla (c. 305[1]), shared with *Brachydelphis mazeasi* and *Stenasodelphis*; intermediate separation between posterior-most point of right premaxilla and nasal (c. 306[1]), shared with *Pontoporia* and *Stenasodelphis*; medial portion of maxilla on either side of the vertex face mainly dorsally (c. 307[2]), shared with *Pontoporia* and

Pliopontos; longest side of nasal facing anterodorsally (c. 311[1]), shared with all inioids except *Pontoporia* (face dorsally: c. 311[0]), and *Ischyrorhynchus* and *Inia* (face anteriorly: c. 311[2]).

Among pan-iniids, [redacted] shares with *Meherrinia* and *Inia* (not preserved in *Ischyrorhyncus*) three or more dorsal infraorbital foramina (c. 64[2]); with *Ischyrorhynchus*: premaxillae on anterior two thirds of rostrum contact along the midline for nearly their entire length (c. 9[0]), tooth enamel with reticular striae (c. 26[1]), anterior edge of nasals in line with posterior half of supraorbital processes (c. 80[4]); shares with *Inia* and *Ischyrorhynchus* supraorbital processes of frontal that slope laterodorsally away from vertex (c. 46 [2]), transverse width of nasals within 10% of nares width (c. 119[2]), nasals elevated above rostrum relative to lateral edge of maxilla (c. 123[1]), frontals higher than nasals (c. 124[2]). Shares with *Inia* the following synapomorphies: posterior buccal teeth that are nearly an equilateral triangle (c. 30 [1]), small lacrimal (c. 50[0]), small exposure of the lacrimal and jugal posterior to the antorbital notch (c. 55[0]), posterior portion of nasals elevated above rostrum (c. 123[1]), frontals posterior to nasals with same width as nasals (c. 125[1]), maxilla on dorsal surface of skull does not contact supraoccipital posteriorly (c. 129[0]), dorsal edge of zygomatic process with distinct dorsal flange (c. 143[1]).

Lastly, *Carbinia* displays the following apomorphies: maxilla and premaxilla fused along most of rostrum (c. 10[0]), lower number of mandibular teeth (18) (c. 37[5]), dorsal edge of orbit low relative to lateral edge of rostrum (c. 47[1]), premaxilla is convex transversely anterior to nasal openings (c. 68[1]), posterior-most end of ascending process of premaxilla in line with posterior half of supraorbital process of frontal (c. 74[2]), very narrow width of posterior edge of nasals (c. 120[3]), slight emargination of posterior edge of zygomatic process by sternomastoid muscle fossa (c. 144[1]), dental roots that are elongate, rugose, bulbous, and much larger than the tooth crowns, with some roots that

have their apices oriented posteriorly so that they come close to the anterior end of the root of the succeeding tooth.

Etymology. Honors a family dedicated to exploring the natural world, whose curiosity will lead to new discoveries, far into the future.

Description

Skull

The skull of [redacted] is relatively complete on its dorsal aspect, although it is missing the left side of the facial bones (Figure 3). The skull is heavily eroded along its ventral surface, and the basicranium is absent except for a small portion of the right parietal and right alisphenoid (Figure 4). The skull preserves most of the dorsal aspect of the supraoccipital, including small portions that articulate with the vertex and nuchal and sigmoidal crests (Figure 3A-C). Overall, the profile of the skull is dominated by the rostrum, which is complete and comprises approximately 75% of the length of the preserved skull (the rostrum length is 36.6 cm; Table 1). The anterior portion of the rostrum is slightly displaced by both an oblique and transverse fractures, likely from geologic compaction or other diagenetic factors, which displace the elements approximately 1-2 mm from their life positions. Most of the upper dentition is missing from the skull, except for the anterior teeth, some of which are complete; other more posterior teeth are incomplete, while three isolated teeth were recovered from the quarry at the type locality. Despite the heavy erosion that removed most of the left portion of this skull, sufficient anatomical details are preserved on the right side of the cranium, and along the rostrum to provide insights into the morphology of [redacted]

Premaxilla. In dorsal view, the premaxilla dominates the visible part of the rostrum, comprising the entirety of the rostrum from its anterior end to about 75% of the length of the rostrum. In this view, the premaxilla occupies a width greater than that of the maxilla until the level of the maxillary flange (*sensu* Mead & Fordyce, 2009: 62), where the width of the premaxilla begins to taper relative to the expansion of the maxilla overlying the cranium, in dorsal view (Figure 3). Along the rostrum, anterior of the premaxilla-maxilla suture, there are several shallow canals that terminate in small oval foramina (~5 mm long by ~2 mm wide). These canals are similar to those observed in adult specimens of *Inia*, but markedly different from the singular, deep groove that separates the posterior connection of the premaxilla and maxilla in *Pontoporia, Ischyrorhynchus,* immature specimens of *Inia*, and *Lipotes*. In both [redacted] adult *Inia* and *Lipotes*, these canals disappear posteriorly, as the premaxilla-maxilla suture becomes seamless along the length of the rostrum.

The paired right and left premaxillae are unfused for 4 cm at their anterior tip (Figure 3A,B,D), presenting a slight gap, which is likely homologous in other odontocete taxa with the mesorostral groove (sensu Mead and Fordyce, 2009:16). This gap is then obscured posteriorly by full sutural fusion between the premaxillae for 24 cm along the midline of the rostrum until an elongate (6.9 cm-long) window is exposed between the overarching right and left premaxillae, just anterior of the level of the antorbital notches (Figure 3A,B). Near the anterior origin of this window, the anteromedial sulcus appears, approximately at the transverse level of the last upper tooth alveolus (Figure 4). This latter sulcus extends subparallel to the latter window until it terminates posteriorly in the premaxillary foramen. In *Inia*, the anteromedial sulcus extends farther anteriorly, and the portion of the premaxilla medial to the sulcus is more bulbous, while in *Pontoporia* the anteromedial sulcus is deeper, and nearly enclosed dorsally by overhanging flanges of the premaxilla. Fossil pontoporiids show a broadly similar to *Pontoporia*, whereas in fossil iniids, such as *Ischyrorhynchus* and *Meherrinia*, this area is not well

preserved. At the level of the premaxillary foramen, the right and left premaxillae diverge from their midline fusion in separate paths around the external bony naris. This divergence produces a V-shaped gap, 32 mm in anteroposterior length and 9 mm in lateral width, which is narrowed and longer than fossil pontoporiids, such as *Auroracetus*; this gap is small and variable in *Inia*, and broad and triangular in *Ischyrorhynchus* and *Meherrinia*.

The premaxillary foramen itself is thinly ovate, 11 mm anteroposterior length, and 4 mm wide, unlike the small, subcircular foramina in pontoporiids and other iniids. (The left side of the cranium, from this level posteriorly is not preserved, and thus the remainder of the description necessarily uses the right side of the cranium). The posterolateral sulcus is shallow, and extends slightly laterally from its deepest portion at its origin, the premaxillary foramen. The posterolateral sulcus terminates posteriorly in a faint way at the level of the anterior margin of the external naris. This condition is similar to *Meherrinia* and *Brachydelphis,* while it is different from *Pontoporia, Auroracetus, Pliopontos*, *Pontistes* and *Inia*, which present a deeply excavated sulcus along the posterolateral edge of the premaxilla. This portion of the premaxilla is not well preserved in *Ischyrorhynchus*. Medially, the posteromedial sulcus is unusual in originating 9 mm posterior of the premaxillary foramen and bifurcating into lateral and medial tracts that delineate the borders of the premaxillary sac fossa. Along with the posterolateral sulcus, these bifurcating tracts create a Z-shaped sulci pattern that is shallow laterally and deep (>3 mm) anteromedially. The path of medial tract of the posteromedial sulcus extends along the lateral margin of the anterior half of the external naris, but it is not confluent with the border of the naris. This morphology is completely new, and not observed in any inioid nor delphinidan. The bifurcating tracts enclose a low, but convex premaxillary sac fossa located lateral to the external naris and dipping medially, whereas the premaxillary sac fossa in all other inioids is located anterolateral of the external naris and is strongly convex, except for *Meherrinia* and

Pliopontos. This portion is not preserved in *Ischyrorhynchus.* The premaxillary sac fossa in *Lipotes* is flat, with elevated margins.

The patent posterior termination of the entire premaxilla is spatulate, flat, and it appears at the level of the posterior half of the external bony naris, as in *Meherrinia*. There is an 8 mm separation between the posteomedial termination of the premaxilla and the anterolateral-most point of the nasal. In contrast, the posterior termination of the premaxillae of *Pontoporia* reaches the level of the posterior edge of the external nares, while in adult *Brachydelphis* spp., *Pliopontos*, *Pontistes*, *Inia*, and *Lipotes*, it extends even farther posteriorly, meanwhile in young specimens of *Brachydelphis* and *Pontoporia* it is in an intermediate position. Although there is slight erosion of the bony surface along the immediate margin of the external naris, the gap between the premaxilla and nasal is patent.

Maxilla. Throughout most of the anterior two thirds of the rostrum, the maxillae and premaxillae have a cylindrical outline (Figure 3). Dorsally, the maxilla is exposed slightly on the lateral margin of the rostrum that is otherwise dominated by the premaxilla until about the proximal third of the rostrum where the maxilla becomes flatter along the maxillary flange. (As with the premaxilla, nearly all of the facial portion of the left maxilla has been lost to erosion, and the description is based on the right side). The antorbital notch is widely open, U-shaped, and oriented anteriorly. Posterior to the antorbital notch, the maxilla is expanded to cover most of the supraorbital process of the frontal, with the exception of the posterior-most and posteromedial edge, where the frontal is exposed. This posteromedial exposure of the frontal is similar to the condition observed in *Ischyrorhynchus* and *Inia* (mainly in juveniles), and differs from *Pontoporia, Pontistes, Pliopontos, Meherrinia, Brachydelphis* spp., and *Lipotes*, where the maxillae reaches the nuchal crest, and the lateral edges of the vertex. Posterolateral to the antorbital notch, the maxilla form a low maxillary crest (*sensu* Mead & Fordyce,

2009:51), which extends from the preorbital process, continues along the length of the supraorbital process of the frontal, but terminates at the postorbital process, unlike in *Inia*, where the crest continues well posterior of the postorbital process and join the temporal crest. In [redacted] the maxillary crest is mediolaterally thicker (2-6 mm), but lower (~ 5 mm), than the thinner, but higher (> 5 mm) crest observed in *Inia*; in *Pontoporia* and *Pliopontos* this crest extends only the length of the supraorbital process.

Dorsally, the right maxilla shows a large diameter (~10 mm) anterior dorsal infraorbital foramen, located at the level of the antorbital notch (Figure 3A,B,D). A second, anterior dorsal infraorbital foramen is found posterolateral to the first, and it is smaller in diameter (~ 7 mm), and oriented posterolaterally. A single, posterior dorsal infraorbital foramen is located posterolateral to the external nares, it has a diameter of about 9 mm and its orientation is posterodorsal. The posterior dorsal infraorbital foramen of [redacted] is absolutely larger and located farther posteriorly than the corresponding foramen in *Inia, Ischyrorhynchus, Meherrinia, Brachydelphis, Pontistes, Pliopontos, Pontoporia*, and *Lipotes*.

In ventral view, the rostral portion of the maxilla bears alveoli for at least 14 maxillary teeth, with thin interalveolar septa (Figure 4). At the ventral midline contact between the maxillae, there is a longitudinal groove that extends from anteriorly to about the level of the fifth maxillary tooth; a similar sulcus is also observed in *Inia, Pontoporia* whereas this groove reveals a palatal exposure of premaxilla and/or vomer in *Ischyrorhynchus* and *Brachydelphis mazeasi*. Along the ventral surface and anteromedial to the jugal, there is a shallow (~ 2 mm) oval (~ 17 mm long by 10 mm wide) fossa; a similar fossa is also present in some specimens of *Inia, Ischyrorhynchus*, *Brachydelphis* spp. and very slightly *Pontoporia*. Medial to this shallow fossa, there is an elongated fossa that continues anteriorly

parasagittally for about 60 mm, and 5 mm in width and depth. The location and morphology of the fossa corresponds to the anterior sinus of *Inia* (Fraser & Purves, 1960), and it is exposed in [redacted] because its overlying maxilla and palatine were eroded. An anterior sinus is also found in *Ischyrorynchus*, however it is shorter than that in *Inia* and [redacted] The rostral portion is not preserved in the other genera of inioids, preventing any comparison.

Lacrimal and Jugal. The lacrimal appears to be ankylosed with the anterior margin on the supraorbital process of the frontral, forming its anterior surface, a condition common to all adult inioid specimens (Figure 3-5). Ventrally, the lacrimal extends medially to join the jugal, which together forms the anteroventral surface of the antorbital notch. The preserved part of the jugal is a thin strut that is subcylindrical in outline (~4 mm wide; 17 mm long; ~2 mm thick) and oriented posteroventrally. Overall, it is very similar in morphology to the jugal of *Inia*.

Frontal. Dorsally the frontal is mostly covered by the maxilla, but it is exposed along the posterior and posteromedial edges of the skull roof. In [redacted] the right and left frontals form the highest part of the vertex, and together form a pair of rounded, rectangular knobs with a slight midline cleft (Figure 3A-C, 5). This topographic high for the frontals at the vertex is similar in *Inia, Ischyrorhynchus* or *Meherrinia*, and even *Pontoporia* and *Lipotes*, although the frontals in [redacted] are small and low by comparison with pan-iniids. Unlike *Inia* and *Meherrinia*, the midline cleft between the right and the left frontals at the vertex does not show participation of an anterior supraoccipital (or possibly interparietal) wedge externally nor in internal CT scan data (Figure 6). The dorsal surface of the vertex is lightly rugose, but not as strongly as in adult specimens of *Inia*.

The supraorbital process is dorsoventrally thin (~5 mm) with a blunt preorbital process; in contrast, the postorbital process is more elongated with a triangular cross section, similar to the general condition of the other inioids. Nevertheless the distance between this two processes (52 mm), reflecting the size of the orbit is about twice that of adult specimens of *Inia*, but in [redacted] is proportionally similar to the other fossil inioids (all known specimens of *Ischyrorhynchus* lack this feature); see Table 3. In dorsal view, the lateral edge of the supraorbital process is relatively straight and oriented parasagitally, unlike *Inia* and *Pontoporia* where this border is laterally concave and oriented anterolaterally, or the nearly straight but anterolaterally oriented borders of *Pliopontos* and *Brachydelphis*. Additionally, the postorbital process is shorter than the length of the orbit, contrasting with the much longer process and smaller orbit in *Inia*. The ventral surface of the supraorbital processes is gently concave with a low, but distinct postorbital ridge. Medially and posterior to the frontal groove there is a shallow (<1 cm) round (~1.5 cm diameter) fossa for the postorbital lobe of the pterygoid sinus. This same fossa varies tremendously in adult specimens of *Inia*, where it can either be shallow and slit-like (e.g., USNM 49582) or form a deep pit (e.g., USNM 239667). By contrast, this fossa in *Pontoporia* is deep, rounded and floored posteroventrally by the alisphenoid; in *Brachydelphis* spp., this fossa is shallow, as it is in *Lipotes*.

Nasal. The right and left nasals are paired at the vertex, sloping away from the topographic high of the paired frontals (Figures 3,5,6). Overall, the nasal is large (width = ~12 mm; length = 41 mm), dominating the anterodorsal surface of the vertex, and occupying the entire posterodorsal margin of the external bony naris. The anterior margin of nasal is concave. Together, the right and left nasals are anteroposteriorly elongate with some tapering posteriorly, as in *Pontoporia*, *Brachydelphis*, *Pontistes*, *Auroracetus*, *Pliopontos*. However, the nasal in [redacted] is dorsoventrally more massive than these

latter genera, and it is not as anterodorsally inclined as in *Meherrinia* not as anterior-facing as in *Ischyrorhynchus*, *Inia*, and *Lipotes*.

The anterior margin of the nasal displays a low sigmoidal crest that extends transversely with a small protuberance that rises in the middle of the nasal, about 10 mm from its anterior margin; with the paired right and left nasals, these small crests and the base of these protuberances outline a wide, but shallow V-shaped concavity, pointing posteriorly (Figure 3A,B,D). The posterior margin of the nasal is difficult to resolve without close inspection because the sutural distinction between the nasal and the frontal in this part of the vertex is overlapping and thin (see also Figure 6). The posterior termination of the nasal overlaps with the frontal by passing in a broadly posteromedial path, terminating anterior of the level of the posteriormost margin of the maxilla. Together, the posterior termination of the right and left nasals show an anteriorly-pointed V-shaped margin. This condition is similar to *Pontoporia* and *Brachydelphis*, where the contact between the nasal and frontal shows a similar V-shaped margin; in *Auroracetus* and *Meherrinia*, a small wedge of the frontals insert medially between the nasals.

Vomer and Ethmoid. The vomer is poorly preserved ventrally, but a small portion is patent along the midline palatal surface adjacent to the medial margin of the highly eroded right maxilla, approximately extending 45 mm, with an anterior extent to the transverse level of the 8th maxillary tooth alveolus (Figure 4). The ethmoid is incompletely preserved; the crista galli is shallow with very small (<1 mm) foramina in its surface. The ethmoid forms the bony nasal septum, rising dorsally to the same horizontal level as the premaxillae, but not quite reaching the level of the nasals. The lateral wings form the posterior and posterolateral walls of the external nares, which are cleanly separated from the anterior margin of the nasals by a continuous gap 5-8 mm wide.

Parietal. The parietal is exposed broadly on the posterior margin of the temporal fossa, along with the frontal and squamosal (Figures 3C,D, 5). The lateral surface of the parietal is smooth and convex; in posterior view, the temporal crest of the parietal is posterolaterally oriented temporal crest, as opposed to the ventrally oriented crests in *Inia* and *Pontoporia*. The anterior extent of the parietal is unclear because the parieto-frontal suture is not patent, similar to adult specimens of *Inia*.

Supraoccipital. Only the dorsal half of the supraoccipital can be reliably determined for [redacted] Dorsally, the supraoccipital does not participate in the vertex, but participates in the temporal and nuchal crests (Figure 3A-C); the nuchal crest is transversely straight, about 10 mm thick, and unlike the more anteromedially oriented crest in *Inia* and the posteriorly concave crest of *Pontoporia*. Posteriorly, there is a midline sagittal crest that is bounded laterally by deep (9 mm) semilunar fossae; such fossae are also patent in adult specimens of *Inia* and *Pontoporia*. The external surface is smooth and convex. The temporal crests are nearly vertical, and dorsally they join the nuchal and orbitotemporal crests (sensu Fordyce 2002:194), forming a tabular, triangular surface at the triple junction. When viewed posteriorly, the supraoccipital has a square outline, unlike the more sub-triangular outline in *Inia*, or the general pentagonal outlines of *Pontoporia* and *Lipotes*.

Squamosal. The right squamosal is nearly completely preserved. The zygomatic process of the squamosal is relatively long, mediolaterally thin, laterally convex and medially concave. Its anterior edge is squared-off, more like *Inia*, and to a lesser degree *Brachydelphis mazeasi*, rather than the rounded, tapering lateral profile of *Pontoporia and Pliopontos*. The dorsal surface of the root of the zygomatic process is concave, while its lateral edge flares outward about 10 mm farther laterally than the anterior part of the process (Figures 3-5). Ventrally, the outline of the glenoid fossa is elongate, shallowly convex, and faces ventromedially. The tympanosquamosal recess extends as a deep (~5 mm)

sulcus medial to the glenoid fossa. The posterolateral surface of the squamosal has a broad and relatively deep concave sternomastoid fossa, deeper than *Inia*.

The squamosal plate is relatively low, occupying only about the lower quarter of the surface of the temporal fossa, which is dominated by the parietal (Figure 5). This configuration is similar to the condition seen in *Pontoporia* and *Brachydelphis*, but contrasts with *Inia*, where the squamous portion is much higher, a condition also visible in *Lipotes*. The anterior extent of the squamosal plate is ankylosed with the posteroventral edge of the temporal wall exposure of the alisphenoid in the type specimen of [redacted]

Alisphenoid. Only the dorsal portion of the alisphenoid is preserved in the type specimen of [redacted] above the horizontal level the squamosal fossa (Figure 5). In lateral view, the parieto-alisphenoid suture extends in a path from the squamosal plate at the posterior margin of the temporal fossa dorsally to a level in line with the nuchal crests; in this way, this sigmoidal suture partitions the parietal (dorsally) and the alisphenoid (ventrally) in the middle of the temporal fossa. The anterior margin of the alisphenoid extends at least to the level of the postorbital processes of the frontal, although the actual sutures are not patent at the anterior end. In lateral view, the dorsal extent of the alisphenoid on the temporal wall is much greater than that seen in *Inia*, but we note a degree of variability in *Inia*.

Mandible

Both right and left mandibles are preserved intact and remain articulated via an osseous symphyseal articulation (Figures 7-8; Class IV jaw joint of Scapino, 1981). The length of the mandibular symphysis (21.0 cm) is approximately 43% of the entire length of the mandible. The mandibles possess nearly all of the original lower teeth; the lower first incisors are missing, along with posterior most

three teeth of the right mandible (although one isolated tooth is a perfect fit for PC_{12}; see Figure 9E). Both the right and left mandibles possessed 18 lower teeth in life. Although the posterior terminations are missing both angular processes of the mandible, there a weak suggestion of the osteological structure where the left articular condyle would have been. The right articular condyle is missing. Most of the mandibles are well preserved, although much of the right acoustic window is degraded from erosion and/or diagenesis (Figure 8).

In anterior view and posterior views (Figure 7C,D), the mandibles show slight asymmetry in the relative directions of the overall mandibular rami, with the right ramus extending laterally and slightly ventral relative to the left one. This asymmetry may be diagenetic and related to sediment compaction, but we think it more likely records the original right-left asymmetry that is common in other living inioids (Werth, 2006), and this condition is evident in adult specimens of *Pontoporia*, with its proportionally elongate rostrum. In ventral view, the anterior termination of the mandibles from the gnathion to pognion is gradual and not acute, with a ventral outline that is somewhat rectangular. Anteriorly, this termination is flat and not acute. Posteriorly, the ventral surface of the mandibles is U-shaped, in transverse section, through the symphysis. Generally, this morphology is most similar to that of *Inia*, and *Saurocetes argentinus*, which is only known from a mandibular fragment that is less complete than [redacted] (Cozzuol, 2010). The general lateral and horizontal profiles of the mandible in [redacted] are unlike *Pontoporia*, with a deep lateral groove, and unlike the strongly convex mandibles of *Brachydelphis mazeasi* (based on MUSM 887).

The ventral margins of the mandible, posterior of the symphysis, are rounded until the posterior half of the level of the acoustic window when this margin gradually gains an edge (Figure 7D). The medial profile of the acoustic window in [redacted] is dorsoventrally narrower than that of *Inia*, and

considerably more acute than *Pontoporia*. Both right and left mandibles show approximately 7 mental foramina each, spaced along the ventrolateral margins of the mandibles along the symphysis. In each case, the foramina open anteriorly, often forming sulci with long tails. The anterior most foramina are paired close to the midline of the symphysis at the level in between the third and fourth lower tooth. [redacted] shares a high number of mental foramina with Inia, whereas both *Pontoporia* and *Brachydelphis mazeasi* shows fewer (1-2 mental foramina in adult specimens of *Pontoporia*, and 4 mental foramina in MUSM 887).

The overall morphology of the mandibles in [redacted] shares the most similarities with *Inia*, among inioids and delphindans for which this element is known, especially in lateral and horizontal profiles anterior to the symphysis. Posterior of the symphysis, the rami of the mandibles are lower than *Inia*, and slightly more gracile. The mandibles of [redacted] are also not dorsoventrally flattened like those of *Pelodelphis* or *Pomatodelphis*, nor are they slender like those of *Kentriodon pernix* (USNM 8060) and *Brachydelphis mazeasi* (based on MUSM 887). The mandibles of [redacted] differs strongly from *Lipotes*, and fossil delphindans such as *Lophocetus pappus* (USNM 15985) and *Hadrodelphis calvertensis* (USNM 23408 and USNM 189423), which all notably have many more teeth posterior of the symphysis, and exhibit rounded, nearly circular alveoli. Ovate alveoli are notable in putative inioids represented by fragmentary mandibles, such as *Saurocetes argentinus* and *Hesperocetus californicus*, although the dentition of [redacted] is far less bulbous than either. In *Goniodelphis hudsoni*, another putative inioid, the mandibles are relatively deeper, and mediolaterally flattened, with a much longer symphysis, and mediolaterally flattened teeth that are triangular in outline when viewed laterally. The crowns are much more slender and somewhat recurved (see below).

Dentition

Upper. The upper dentition consists of 15 teeth per side, counted by alveoli in the premaxilla and maxilla on the right side of the skull. It is less complete than the lower dentition. Of the original upper dentition, only a total of 14 teeth remain preserved in their alveoli, with 6 in the left side and 8 in the right. Of these intact teeth, the right side preserves only the 2 distalmost teeth with crowns, while the others only preserve the tooth roots, with fractures at the base of the crown that are probably postmortem. An isolated upper right tooth discovered during excavation fits well in the third postcanine (PC^3) alveolus, and the lack of any preserved alveoli posterior to this level increases the likelihood of this placement being correct, although there is no way to eliminate a more posterior placement (see Figure 9F). Another isolated tooth root lacking the crown likely belongs to a right alveolus in the posteriormost dentition that is not preserved on this side of the skull. The left side preserves intact teeth, with crowns, from the first incisor (I^1) to PC^1 and then an open alveolus at PC^2, followed by two tooth roots with rounded breaks where crowns were likely present prior to death. PC^7 is intact, although all of the other alveoli on this side are missing their teeth.

Overall, the teeth have slightly anteroposteriorly expanded tooth roots, exhibiting an ovate outline in occlusal profile at the margin of the alveolus, which is very similar to *Goniodelphis*, *Hesperocetus* and *Ischyrorhynchus*, although [redacted] has more clearly ovate tooth alveoli than all of these. By comparison, *Inia* and *Lipotes* have subcircular tooth outlines at the alveolar margins, whereas *Pontoporia* show nearly rectangular outlines. The posterior roots of the upper teeth are somewhat gibbous, with closed pulp cavities distally. The exposed base of the tooth roots, ventral of the level of alveolar margin, tapers dramatically towards the base of the tooth crown, with the crown situated more or less centrally on the tooth root, except for the anteriormost pairs of incisors, which are slightly procumbent. The base of the upper tooth crowns range from 11-12 mm in diameter, with very light longitudinal striae that surround the perimeter of the base (such light striations are visible on both

lower and upper teeth). The enamelocementum boundary between the roots and the crown is distinct and sharp for both upper and lower teeth. The apices of the upper tooth crowns are worn, leaving subcircular tooth wear outlines through the enamel into the dentin that is polished. With the exception of the first incisors, the crowns of the upper dentition exhibit a slight buccal curve. Wear facets can be noted on the posterior margins at the base of the tooth crown in the first incisors and on the anterior side of PC^1.

Lower. The lower dentition is nearly complete, consisting of 18 teeth per side, and missing only the first lower incisors and the two posteriormost left postcanine teeth. An isolated lower left tooth found during discovery quarrying fits reasonably well in the left PC_{12} alveolus, and the morphology and wear on the tooth crown matches its intact right counterpart (see Figure 9E). Like the upper dentition, the lower teeth posterior of the incisors are broadly ovate in occlusal profile, formed by the margins of the alveoli.

The near complete lower dentition provides detailed information about the morphology of the tooth crowns throughout the mandible for which the upper dentition only provides limited information. While the lateral profile of the lower dentition shows that the teeth are generally oriented vertically, but viewed along the major axis of the mandible, the anterior teeth from the canine (C_1) to PC_3 show buccal curvatures with slight lateral compression and mesiodistal keels that grade into straighter teeth without mesiodistal keels posterior of PC_3 and that also have more apical tooth wear, leaving less of the original tooth crowns. Generally, lower dentition posterior of PC_3 are rounder in occlusal profile, with slight lingual protuberances on the crown beginning at PC_6 that become more patent as true lingual cusps posterior of PC_9. After this level, the lower teeth grade slowly to presenting a more lingual orientation. Posterior of the termination of the mandibular symphysis, the diastemata shorten between adjacent lower teeth, although there is still enough space between the posterior most teeth to

permit interlocking occlusion with the corresponding upper dentition. Most of the lower teeth lack non-occlusal wear facets, except for the right I_2 and left PC_9.

Careful manual articulation of the lower jaw with the rostrum using full size 3D prints of the type specimen shows that the lower and upper dentition interlock in a precise, alternating way similar to extant odontocetes (e.g., *Tursiops*) with robust dentition. Although both lower teeth and upper teeth have crown base diameters in the same range (11-12 mm in mesiodistal diameter), the slightly shorter lower dentition diastemata provides the space for upper and lower teeth to slide past one another. Unusually, I_{2-3} together pass posterior and anterior of I^{1-2}, respectively, although such imprecise occlusions do occur in other odontocetes, and such a similar pairing in the dentition can be observed in *Inia* (the posterior lower teeth of USNM 49582).

Scapula

Only the right scapula is preserved in the type specimen of [redacted] (Figure 9A-C). In dorsoventral dimensions, the preserved element is 16.8 cm tall, and approximately 15 cm in anteroposterior length. The scapula is incomplete, and the following parts are missing from the type specimen: most of the dorsal margin, and especially most of the anterior aspect; most of the acromion; and the anterior tip of the coracoid process. The posterior margin of the suprascapular border is intact, as well as the glenoid fossa and most of the region surrounding the ventral aspect of the scapula.

The scapula is broadly fan-shaped, although it is exceedingly thin along the broken dorsal border, ranging from 1-3 mm in mediolateral thickness (Figure 9A,B). Nearly the entire part of the scapula housing the supraspinous fossa is missing, and only the basal 2 cm of the spinous process at its L-junction with the base of the acromion is preserved. The infraspinous fossa is deep, and it is the most

concave aspect of the scapular topography in lateral view. Consequently, in medial view, the costal surface of the scapula shows corresponding and marked convexity. The depression for the teres major muscle is shallow, but patent. In dorsal view, the most striking aspect of the scapular morphology is the sinusoidal profile of the dorsal border created by the deep infraspinous fossa.

The acromion is incomplete, but the preserved base shows that it was dorsoventrally tall (25 mm) relative to the same dimension of the coracoid process, thin (4 mm in mediolateral thickness), and curved medially from its base; reminiscent of the condition observed in *Inia*. This morphology differs from the anteriorly rounded, subtriangular outline of the acromion of *Brachydelphis mazeasi* (MUSM 887) and *Pontoporia*, where the proximal end of the acromion is dorsoventrally broad and tapers distally. In lateral view, the angle formed by the acromion and the spinous process in [redacted] is nearly 90 degrees, and the anterior margin of the scapular border bisects this angle at about 70 degrees from the dorsal margin of the acromion. The coracoid is stepped medially from the level of the acromion, and it is thicker laterally than the acromion, with a slight lateral curve, and presents a slightly spatulate anterior termination, which is typical in delphinidans.

The glenoid fossa is 13 mm deep at its deepest, relative to its ventral margins. In ventral view, the overall shape of the glenoid fossa is roughly that of a slightly laterally compressed oval (Figure 9C); when combined with its depth, the overall topography of the glenoid fossa is reminiscent of an ice cream scoop. A sharp posterior margin of the posterior scapular border extends to the margin of the glenoid fossa.

Phylogenetic Analysis

We obtained six most parsimonious trees (length = 1922; consistency index = 0.283, and retention index = 0.451), in our phylogenetic analysis, with the consensus tree shown in Figure 10. The resulting topology of the consensus tree is overall very similar to that obtained by Aguirre-Fernández & Fordyce (2014:fig. 8), with the notable difference that the relationship of *Pontoporia*, *Brachydelphis* and *Pliopontos* with other inioids which is unresolved in our analysis, yielding a polytomy for Pontoporiidae (*sensu* Geisler et al. 2012). Our results also resolved a clade (new name, Pan-Iniidae) of taxa more related to *Inia* than *Pontoporia*, which consists of: *Meherrinia*, *Ischyrorhynchus* and [redacted] the latter which is sister to *Inia*. Although Bremer support values for most of these nodes is low (i.e., 1 step), there is stronger support (i.e., 2 steps) for the clade that includes *Ischyrorhynchus*+[redacted]*Inia*. The new position of *Ischyrorhynchus* within Pan-Iniidae is likely a result of our rescoring of several characters based on observations of the type and additional specimens of *Ischyrorhynchus*. This position differs from all previous phylogenetic analyses (e.g., Geisler et al., 2012; Aguirre-Fernández & Fordyce, 2014) but it is consistent with Cozzuol (2010)'s proposal for a subfamily grouping of Ischyrorhynchinae within Iniidae (Cozzuol, 1996). Our analysis did not include *Saurocetes* spp., a large fossil iniid known from the late Miocene age Ituzaingó Formation of Argentina and Solimões Fm. of Brazil, and represented mainly by fragmentary mandibular remains (Cozzuol, 1996; Cozzuol, 2010). We also did not include *Goniodelphis hudsoni* from the Mio-Pliocene age Bone Valley Formation of Florida (Allen, 1941), which is represented by a poorly preserved cranium with some similarities to *Ischyrorhynchus*. Both taxa require reexamination that remains outside the scope of this study.

Our results differ in resolving a clade grouping of *Lipotes*, *Platanista* and extinct lipotid *Parapontoporia* spp., which shares some similarities with Platanistoidea *sensu* Simpson (1945) and Geisler and Sanders (2003). The recovery of *Platanista* in a close relationship with other lipotids has

been a frequent result of exclusively morphological analyses, whereas exclusively molecular and combined molecular and morphological analyses consistently recover *Platanista* as a separate, basal branching clade from *Lipotes* and Inioidea, likely reflecting long branch attraction. Regardless, both morphological and molecular (and combined) analyses have consistently recovered Inioidea as a clade (i.e., *Inia* and *Pontoporia*), a finding replicated by our own results, herein.

Discussion

1. [redacted] compared with other living and extinct inioids

Among inioids, the general morphology of [redacted] in dorsal view most resembles the known elements of *Meherrinia* and *Inia*; in ventral view, it is most similar to *Ischyrorhynchus* and *Goniodelphis*, although both of these taxa are represented by more fragmentary remains than [redacted] The rostrum of [redacted] is robust, with dorsal fusion between the right and left premaxillae, and possessing relatively robust upper and lower dentition, with strong wear on the apical crowns, although [redacted] does not exhibit lingual cusps in the posterior dentition observed in *Inia*. Additionally, tooth counts are more similar to *Inia*. The strong groove separating the premaxilla and maxilla along the length of the rostrum is most similar to *Inia*, whereas *Pontoporia* and *Ischyrorhynchus* show a small but deep indentation that runs the length of the rostrum. In some ways, the rostrum of [redacted] is reminiscent of *Kampholophos serrulus*, from the late Miocene of California (Rensberger, 1969), which is likely a pan-iniid-mimic delphinoid, although the dentition of [redacted] is far less crenulated.

[redacted] exhibits a large dorsal infraorbital foramen on the maxilla, which is proportionally similar to *Inia* and *Ischyrorhynchus*, although absolutely larger in [redacted] In ventral view, [redacted] shows anteriorly elongate anterior sinus system, invading the maxilla, a feature observed also in *Inia* (Fraser

& Purves, 1960). Overall, the lateral profile of the rostrum in [redacted] remains in the same level as the cranium, whereas both *Pontoporia* and *Inia* shows a slightly dorsal elevation of orbits, a featured most pronounced among odontocetes in *Lipotes*. Using the small crest on the supraoccipital as an external demarcation of the hemispherical midline of the underlying dermocranium, we note that the vertex in [redacted] is slightly sinistral, to the same degree as *Inia*, and more so than *Pontoporia*, although not as highly sinistral as *Lipotes*. Interestingly, [redacted] lacks the strongly elevated and knob-like vertex of *Inia* and *Ischyrorhynchus*, maintaining a lower profile of *Meherrinia* and *Pontoporia*, although its frontals do form the absolutely apex just as they do in *Inia*, with a pedestal that can be directly pinched between an index finger and thumb, anterior of the apex of the supraoccipital shield. Notably, [redacted] lacks the strongly inflated bosses of the premaxillary sac fossae seen in nearly all other inioids.

The mandible of [redacted] is most similar to *Inia*, in terms of an elongate mandibular symphysis, morphology in transverse section, and general size. Both [redacted] and *Inia* lack the distinct ventrolateral groove in *Pontoporia*. Mental foramina with overhanging sulci are prominent in [redacted] but smaller in *Inia*, although in both they extend posteriorly along the body of the ramus; also, the anterior termination of the mandibles in [redacted] is rounded in lateral view, whereas it is more angular in *Inia*. In lateral view, the coronoid process in [redacted] is less elevated, relative to the level of the trough in the mandibular symphysis than either *Inia* or *Pontoporia*. Both in [redacted] and *Inia*, the posterior termination of the dentition and the anterior termination of the acoustic window occur in close proximity, whereas in *Pontoporia* these landmarks are separated by a large gap along the mandibular ramus. Lastly, for the scapula, [redacted] shares the most similarities with *Inia*, although the scapula is not known in the majority of fossil inioids, and it remains unpublished in the otherwise abundantly represented *Brachydelphis mazeasi* (e.g., MUSM 887). We note the presence of both a

complete scapula and a humerus in the type specimen of *Incacetus broggii* (AMNH 32656). The pan-iniid-like features of both elements hinting at inioid affinities for this taxon, from the Pisco Basin of Peru, which has previously been identified as a kentriodontid (Muizon, 1988b).

2. Taphonomy, body size, and ecomorphology

[redacted] was recovered from the type locality with the ventral surface of the skull exposed stratigraphic up, at the outcrop surface, directly overlying the mandibles, which were preserved slightly askew from the main axis of the skull, dorsal surface up. Careful inspection of the surrounding quarry, prior to excavation, led to the recovery of 3 isolated teeth. The scapula was recovered within 1 meter of the skull and jaws, mid-way through the excavation. This degree of disarticulation corresponds to Articulation Stage 2 described by Pyenson et al. (2014b) in their supplemental files, which matches the same articulation stage in Boessenecker et al. (2014). In terms of bone modification, there is no evidence of bite marks from marine macroscavengers, and we did not observe any of the phosphatization, fragmentation and polish described by Boessenecker et al. (2014) for marine vertebrates from the Mio-Pliocene age Purisima Formation of California. In sum, these observations point to the type specimen of [redacted] representing a single individual skeleton showing little transport, slight disarticulation, and buried in a low energy depositional environment.

Using both the Platanistoidea and Delphinoidea body size equations from Pyenson & Sponberg (2011), we calculated the total length of [redacted] between 284-287 cm, respectively, based on an estimate of the bizygomatic width of the skull by doubling the distance from the lateral surface of the zygomatic process to the midpoint of the mesethmoid. Assuming the type specimen represents a mature individual, this total length exceeds the largest values for *Inia* (LACM 19590 with TL = 221 cm) and *Pontoporia* (CAS 16529, with TL = 157 cm) from the adult specimens cited in Pyenson & Sponberg

(2011)'s dataset. The reconstruction of [redacted] TL closely matches medium to large size extant delphinoids, such as *Grampus griseus*, which has an average TL of 283 cm, based on 8 adult specimens in Pyenson & Sponberg (2011)'s dataset. Notably, [redacted] ranks among the largest of inioids, though slightly smaller than a similar estimate for *Ischyrorhynchus* (TL of 288-291 cm based on MACN 15135). *Saurocetes* spp., a pan-iniid taxon, was likely much larger, but it poorly known, based on incomplete material from the Ituzaingo Formation of Argentina for *Saurocetes gigas* (only known from a proximal fragment of a mandibular symphysis and isolated teeth), and mandibles and partial cranial specimens for *S. argentinus* from the late Miocene Ituzaingó, Urumaco, and Solimões formations of Argentina, Venezuela, and Brazil, respectively (see Gutstein et al., 2014b).

We also examined two relevant morphological ecomorphological indices: mandibular bluntness index (MBI) and proportional orbit size. First, we followed methods outlined by Werth (2006) and calculated a MBI value of 0.548 in [redacted] which is greater than values for either *Inia* or *Pontoporia*. By comparison, the MBI value for [redacted] most closely resembles those for *Lagenorhynchus* spp., reported by Werth (2006). We also generated a simple metric to compare relative orbit size (ROS) among odontocetes, in an effort to better quantify the proportionally large orbits of [redacted] especially with respect to *Inia* and *Pontoporia*. Using antorbital notch width to control for size (following Pyenson & Sponberg, 2011), we calculated a ROS value for [redacted] at 0.40 (Table 3). This value is larger than *Inia*, but smaller than *Meherrinia, Pontoporia*, and *Brachydelphis* spp.

Overall, [redacted] does share some ecomorphological similarities with pelagic odontocetes, especially with delphinioids of comparable body sizes and MBI. The preponderance of occlusal wear facets on the apices of the lower and upper tooth crowns is not dissimilar from extant delphinioids, such as off-shore specimens of *Tursiops*, and fossil delphinidans such as *Lophocetus pappus*, although [redacted]

has different overall tooth morphology and tooth counts as compared with stem and crown delphinoids, yet far fewer teeth than *Inia* and *Pontoporia*. Comparisons among the dimensionless ROS indices do not immediately reveal any strong phylogenetic or ecologic structuring (Table 3), with [redacted] having a ROS in the same range as fossil and living marine odontocetes. It is entirely possible that ROS does not have the same importance in the sensory ecology of odontocetes as it does in other marine mammals that do not echolocate and therefore depend much more on visual prey detection (Schusterman et al., 2000; Debey & Pyenson, 2012).

3. Environmental and ecological implications

Planktotrophy is the dominant feeding mode of both the benthonic and nektonic invertebrate communities preserved in the Piña Facies (Schwarzhans & Aguilera, 2013; O'Dea et al 2007). This situation contrasts with modern Caribbean shelf communities, where most productivity is benthonic on reefs and seagrasses (O'Dea et al. 2007). The high planktonic productivity in the Piña Facies was consistent along the Caribbean coast of Panama during the late Miocene, but fell dramatically when the Isthmus of Panama formed ~3.5 Ma (Jackson & O'Dea 2013). The presence of [redacted] and other predators including billfishes (Fierstine, 1978; JVJ, pers. obs.), and chondrichthyans (Carrillo-Briceño et al., 2015) and cetaceans including kogiids (Velez-Juarbe et al., in press), physeteroids with *Scaldicetus*-like teeth (Vigil & Laurito, 2014), and delphinoids (JVJ pers. obs.), all with presumably high metabolic rates, corroborate further the presence of high planktonic productivity.

The source of high planktonic productivity is not yet resolved. Upwelled, nutrient-rich Pacific waters may have entered the Caribbean coast of Panama (O'Dea et al. 2012) through the remaining straits of the Central American Seaway (Jackson & O'Dea 2013, Coates & Stallard 2013, Leigh et al., 2014) in the late Miocene. High rates of cloning in cupuladriid bryozoans (O'Dea & Jackson 2009), high

variations in stable isotopes along skeletal profiles from gastropod shells (Robbins et al., 2012), and high variations in temperature-mediated zooid sizes (O'Dea et al., 2007) all suggest that strong seasonal upwelling was a dominate regime in this area. Alternatively, nutrients may have originated from more localized terrestrial runoff, as proposed for emergent platforms in present-day Colombia (Montes et al., 2015). However, reconciling the small watershed of the Isthmus of Panama with the geographic and stratigraphic extent of the Piña facies (approximately 40-50 m thick) make it an unlikely that high productivity levels observed throughout the facies could have been maintained solely from terrestrial input, even if higher rainfall and greater orogenic or volcanic activity in the late Miocene led to increased nutrient input from the proto-Isthmus. As such, it is unlikely that there were large rivers close to the area, further corroborating the hypothesis that [redacted] lived in a fully marine habitat.

The high abundance of benthic foraminifera assemblages with modern or ancient upper and middle bathyal depth ranges led Collins et al. (1996) to conclude that the Piña Facies of the Chagres Formation was deposited in deeper waters. Collins et al. (1996) suggested that the Piña Facies were preserved as the Central American Seaway deepened following the deposition of the underlying shallow-water Gatun Formation, and therefore represented the ephemeral formation of a fairly deep oceanic connection from the Pacific Ocean into the Caribbean Sea, prior to final closure of the Isthmus of Panama. This pattern of sediment deepening at the end of the Miocene, followed by shallowing and final closure of the Isthmus in the late Pliocene, repeats itself across several basins along the Isthmus of Panama (Coates et al., 2003; 2004), pointing to pervasive regional eustatic sea level rise at the end of the Miocene (Miller et al., 2005) as a driver.

De Gracia et al. (2012) suggested that the extent of deepening at this time was extreme. They used the vast abundance of lanternfish (e.g., *Diaphus*) recovered from the sediments (Schwarzhans & Aguilera, 2013) as evidence that the Piña Facies was deposited in up to 700 m of water depth (see Supplemental File 2 for otolith abundance data from this unit, near the type locality). Although lanternfish do inhabit deeper waters during the day to avoid predation, they are well known to migrate into shallow waters at night to feed. Indeed, their otoliths are abundant in shallow water (<35 m) sediments in Bocas del Toro today. Thus, the presence of lanternfish, even in the great abundance observed in the Piña Facies is insufficient to assume deep-water deposition.

In a more recent study, Hendy et al. (in press) used molluscan, foraminferal, coral, and fish otolith assemblages, along with detailed sedimentological evidence, to conclude that the deepening event was considerably less pronounced. They suggested the deposition of the Piña Facies was around 125 m in depth, closely reflecting a previous estimate made by Collins et al. (1999) using corals and fish otoliths. Intense productivity or upwelling characteristic of the Piña Facies could have compressed thermoclines and compensation depths resulting in an apparent compression of the depth ranges of diagnostic taxa resulting in possibly anomalously deep estimates. The presence of a single specimen of [redacted] sheds little light on this palaeodepth discussion, except to note that modern day pelagic delphinoids concentrate around the neritic zone (Benoit-Bird & Au, 2003; Gowans et al. 2007; Benoit-Bird & McManus, 2012).

4. The Evolutionary History of Inioidea in the Americas

The fossil record of Inioidea reveals a far broader geographic distribution in the past than would be predicted from the extant ranges of *Inia* and *Pontoporia*. Fossil inioids outside of South America have

predominantly been recovered from marine deposits representing nearshore depositional environments, although [redacted] recovery from rocks representing potentially a open ocean setting is consistent with ecomorphological traits that [redacted] shares with pelagic odontocetes alive today (Figure 11). Although some freshwater fossil pan-iniids from the late Miocene of Argentina may have been ~4 m in total length, they are based on fragmentary remains (Cozzuol, 2010), and [redacted] is the largest marine inioid yet reported, in addition to being the only fossil inioid known from the Caribbean. Based on the available evidence, [redacted] occupied a high trophic level in a highly productive fully marine tropical Caribbean coastal ecosystem that predated the complete formation of the Panamanian Isthmus, and it likely consumed many of the bony fish that are recorded in spectacular abundance from adjacent otolith assemblages (Supplemental File S2).

Hamilton et al. (2001) suggested that the marine ancestors of *Inia*, subsequent to their divergence from *Pontoporia*, invaded the Brazil Craton during eustatic sea-level highs of the middle Miocene, and evolved freshwater habits prior to the subsequent drop in eustatic sea-level late in the Neogene. This proposed evolutionary scenario is entirely consistent with the late Miocene (Tortonian) antiquity of [redacted] which establishes a minimum boundary on its divergence with *Inia* (Figure 12). Fossil remains attributable directly to *Inia* spp. have been reported from Pleistocene age freshwater deposits of the Rio Madeira Formation in Brazil (Cozzuol, 2010). An isolated pan-iniid humerus from the late Miocene Ituzaingo Formation implies that this lineage had already invaded turbid, obstructed shallow rivers and flooded forests typical of today's Amazonian freshwater ecosystems by this time, although this humerus may belong to extinct taxa more closely related to *Ischyrorhynchus* (Gutstein et al., 2014a).

The results of our phylogenetic analysis, however, cast some complexity on a simple scenario of marine-to-freshwater directionality given the phylogenetic placement of *Ischyrorhynchus*, from freshwater deposits of South America. Taken at face value, our analysis points to either two separate freshwater invasions in South America from marine ancestry at different times (one for *Ischyrorhynchus*, and another for *Inia*), or a single invasion with the origin at the unnamed clade of *Ischyrorhynchus* [redacted] *nia*, with a marine re-invasion leading to [redacted] (Figure 12). While the overwhelming marine ancestry for Inioidea is clear from the phylogenetic background of most odontocetes, there is no clear parsimonious argument for the directionality of marine-freshwater ecological transitions. Geisler et al. (2011) discussed such ecological complexity in considering Hamilton et al. (2001)'s scenario, pointing specifically to separate instances of overlapping geographic and ecological distributions between sympatric pairs of exclusively freshwater and estuarine to marine odontocete taxa: e.g., *Inia* and *Sotalia fluviatilis*, a delphinid, in South America (Gutstein et al., 2014b); and *Lipotes* and *Neophocoena*, a phocoenid, in China. These extant examples, along with the recent fossil discoveries of putatively marine odontocetes in freshwater depositional environments (Bianucci et al., 2013; Boessenecker & Poust, 2015) suggest that freshwater invasions by marine odontocetes have happened frequently throughout the Neogene, in different continental margins, across major lineages, and, as our results suggest, perhaps within clades as well.

For South America, we conclude that marine odontocetes likely invaded freshwater ecosystems several times, with platanistids representing an initial invasion in the middle Miocene that ultimately disappeared, prior or subsequent to later a singular or repeated pan-iniid invasion in the late Miocene. Future work, including new discoveries, will hopefully increase branch support for the phylogenetic arrangement of pan-iniids (and basal inioids), and better refine this scenario for South American inioid evolution, and elsewhere. These evolutionary hypotheses may also be compared with diversity and

extinction selectivity patterns for other vertebrate groups that invaded freshwater ecosystems from marine ancestries (e.g., stingrays belonging to Potamotrygonidae, Lovejoy et al., 1998; croakers in the genus *Plagioscion*, Cooke et al., 2011), in conjunction with the timing of orogenetic events in the late Neogene (Hoorn et al., 2010). Lastly, comparative phylogenetic analyses of the physiology and functional morphology of odontocetes, and other possible marine tetrapod analogs, with overlapping ecological occupancy will also provide a better basis for evaluating adaptational hypotheses in their evolutionary history (Kelley & Pyenson, 2015).

Supplemental Information

S1: Character matrix.

S2: Otolith data.

Additional Information and Declarations

Competing Interests

Nicholas D. Pyenson is an Academic Editor for PeerJ.

Author Contributions

Nicholas D. Pyenson, Jorge Vélez-Juarbe, Carolina S. Gutstein, Holly Little, Dioselina Vigil, and Aaron O'Dea conceived and designed the experiments, performed the experiments, analyzed the data, contributed reagents/materials/analysis tools, wrote the paper, prepared figures and/or tables, reviewed drafts of the paper.

Data Deposition

The following information was supplied regarding the deposition of related data: full resolution 3D models and CT data are available online at Smithsonian X 3D: http://3d.si.edu

New Species Registration

The electronic version of this article in Portable Document Format (PDF) will represent a published work according to the International Commission on Zoological Nomenclature (ICZN), and hence the new names contained in the electronic version are effectively published under that Code from the

electronic edition alone. This published work and the nomenclatural acts it contains have been registered in ZooBank, the online registration system for the ICZN. The ZooBank LSIDs (Life Science Identifiers) can be resolved and the associated information viewed through any standard web browser by appending the LSID to the prefix "http://zoobank.org/". The LSID for this publication is: urn:lsid:zoobank.org:pub:4763A625-883D-4263-B376-33B9F9AD56A4. The online version of this work is archived and available from the following digital repositories: PeerJ, PubMed Central and CLOCKSS.

Funding

The research of N.D.P was funded by the Smithsonian Institution, its Remington Kellogg Fund, and with support from the Basis Foundation. This project was partially funded by an NSF EAR Postdoctoral Fellowship (1249920) to J.V.J. Funding from CONICYT, Becas Chile, Departamento de Postgrado y Postítulo of the Vicerrectoría de Asuntos Académicos of Universidad de Chile supported C.S.G. This research was supported financially by the National System of Investigators (SNI) of the National Secretariat for Science, Technology and Innovation of Panama (SENACYT) to A.O. The funders had no role in study design, data collection and analysis, decision to publish, or preparation of the manuscript.

Institutional Abbreviations

AMNH, Division of Paleontology, American Museum of Natural History, New York, New York, U. S. A.

CAS, Department of Birds and Mammals, California Academy of Sciences, San Francisco, California, U.S.A

LACM, Departments of Mammalogy and Vertebrate Paleontology, Natural History Museum of Los Angeles County, Los Angeles, California, U.S.A

MACN, Museo Argentino de Ciencias Naturales "Bernardino Rivadavia," Buenos Aires, Argentina

MLP, Museo de La Plata, La Plata, Argentina.

MUSM, Museo de Historia Natural, Universidad Nacional Mayor San Marcos, Lima, Peru.

USNM, Departments of Paleobiology and Department Vertebrate Zoology (Division of Mammals), National Museum of Natural History, Smithsonian Institution, Washington, D.C., U.S.A.

Acknowledgements

Foremostly, we thank Felix Rodriguez, Owen McMillan and Eldredge Bermingham for their support. We would also like to thank Celideth DeLeon for her circumspect administrative help. We are grateful to the Government of Panama's *Ministerio de Comercio e Industrias* and staff at STRI for assistance with the transport of the type specimen of [redacted] which was collected and exported with permits from the Ministry of Commerce and Industry (MICI). We thank Steve Jabo and Pete Kroehler (USNM) for technical assistance. [We also thank reviewers for comments]. Santosh Jagadeeshan, Andrew Ugan and Carlos De Gracia gave logistical support. For insightful discussions and access to unpublished data, we thank Stephen J. Godfrey, Olivier Lambert, Mizuki Murakami, R. Ewan Fordyce, James G. Mead, Charles W. Potter, David J. Bohaska, and Alexander J. Werth. For assistance in the field, we thank Andrew Ugan and Santosh Jagadeeshan. We also thank Charles W. Potter, John J. Ososky, and James G. Mead (all USNM), Rodolfo S. Gismondi (MUSM), Christine Argot, Guillaume Billet, and Christian de Muizon (all MNHN), and John Flynn, Ruth O'Leary, Nancy B. Simmons and Neil

Duncan (all AMNH), who all provided access to collections under their care. We thank Tatjana Dzambazova (Autodesk), Antonije Velevski and Ralph Wiedemeier for website assistance with the 3D model of [redacted] and Guenter Waibel, Adam Metallo, Vince Rossi, and Jon Blundell of the Smithsonian's Digitization Program Office for their support with 3D digitization. We also thank Tina Tennessen for her timely editorial skills. Orangel Aguilera kindly gave permission to use his fish otolith data from the Chagres Formation. Marcelo Viana and Orangel Aguilera kindly allowed us to use fish images in preliminary drafts of [redacted] reconstruction. We thank Austin Hendy for the base map in Figure 1. Lastly, we thank Julia Molnar for her creative and careful execution on the life reconstructions of [redacted]

References

Abel O. 1905. Les Odontocètes du Boldérien (Miocène supérieur) des environs d'Anvers. *Mémoires du Musée royal d'Histoire naturelle de Belgique* 3: 1-155

Aguirre-Fernández G, Fordyce RE. 2014. *Papahu taitapu*, gen. et sp. nov., an early Miocene stem odontocete (Cetacea) from New Zealand. *Journal of Vertebrate Paleontology* 34:195-210.

Arnason U, Gullberg A, Janke A. 2004. Mitogenomic analyses provide new insights into cetacean origin and evolution. *Gene* 333:27-34.

Allen GM. 1941. A fossil river dolphin from Florida. *Bulletin of the Museum of Comparative Zoology* 89:1-24.

Barnes LG. 1985a. Fossil pontoporiid dolphins (Mammalia: Cetacea) from the Pacific coast of North America. *Contributions in Science* 363:1-34.

Barnes LG. 1985b. The late Miocene dolphin *Pithanodelphis* Abel, 1905 (Cetacea: Kentriodontidae) from California. *Contributions in Science* 367:1-27.

Benoit-Bird KJ, Au WW. 2003. Prey dynamics affect foraging by a pelagic predator (*Stenella longirostris*) over a range of spatial and temporal scales. *Behavioral Ecology and Sociobiology* 53:364-373.

Benoit-Bird KJ, McManus MA. 2012. Bottom-up regulation of a pelagic community through spatial aggregations. *Biology Letters* 8:813-816.

Bianucci G, Lambert O, Salas-Gismondi R, Tejada J, Pujos F, Urbina M, Antoine PO. 2013. A Miocene relative of the Ganges River dolphin (Odontoceti, Platanistidae) from the Amazonian Basin. *Journal of Vertebrate Paleontology* 33: 741-745.

Boessenecker RW, Perry FA, Schmitt JG. 2014. Comparative taphonomy, taphofacies, and bonebeds of the Mio-Pliocene Purisima Formation, central California: Strong physical control on marine vertebrate preservation in shallow marine settings. *PloS ONE 9*:e91419.

Boessenecker RW, Poust AW. 2015. Freshwater occurrence of the extinct dolphin *Parapontoporia* (Cetacea: Lipotidae) from the upper Pliocene nonmarine Tulare Formation of California. *Palaeontology*.

Brisson MJ. 1762. Regnum animale in Classes IX distributum, sive synopsis methodica sistens generalem animalium distributionem in Classes IX, et duarum primarum Classium, Quadrupedum scilicet & Cetaceorum, particulare divisionem in Ordines, Sectiones, Genera, et Species. T. Haak: Paris, 296 pp.

Carrillo-Briceño JD, De Gracia C, Pimiento C, Aguilera OA, Kindlimann R, Santamarina P, Jaramillo C. In press. A new late Miocene chondrichthyan assemblage from the Chagres Formation, Panama. *Journal of South American Earth Sciences* 60:56-70.

Cassens I, Vicario S, Waddell VG, Balchowsky H, Van Belle D, Ding W, Fan C, Lal Mohan RS, Simões-Lopes PC, Bastida R, Meyer A, Stanhope MJ, Milinkovitch MC. 2000. Independent adaptation to riverine habitats allowed survival of ancient cetacean lineages. *Proceedings of the National Academy of Sciences* 97:11343–11347.

Coates AG, Aubry MP, Berggren WA, Collins LS, Kunk M. 2003. Early Neogene history of the Central American arc from Bocas del Toro, western Panama. *Geological Society of America Bulletin* 115:271-287.

Coates AG, Collins LS, Aubry MP, Berggren WA. 2004. The geology of the Darien, Panama, and the late Miocene-Pliocene collision of the Panama arc with northwestern South America. *Geological Society of America Bulletin* 116:1327-1344.

Coates AG, Stallard RF. 2013. How old is the Isthmus of Panama? *Bulletin of Marine Science* 89:801-813.

Cohen KM, Finney SC, Gibbard PL, Fan JX. 2013. The ICS international chronostratigraphic chart. *Episodes* 36:199-204.

Collins LS, Coates AG, Berggren WA, Aubry MP, Zhang J. 1996. The late Miocene Panama isthmian strait. *Geology* 24:687-690.

Collins LS, Aguilera O, Borne PF, Cairns SD. 1999. A paleoenvironmental analysis of the Neogene of Caribbean Panama and Costa Rica using several Phyla. Un análisis paleoambiental del Neogeno del

Caribe de Panamá y Costa Rica utilizando varios Phyla. *Bulletins of American Paleontology* 357:81-87.

Cooke GM, Chao NL, Beheregaray LB. 2012. Marine incursions, cryptic species and ecological diversification in Amazonia: the biogeographic history of the croaker genus *Plagioscion* (Sciaenidae). *Journal of Biogeography* 39:724-738.

Cozzuol MA. 1989. Una nueva especie de *Saurodelphis* Burmeiter, 1891 (Cetácea: Iniidae) del "Mesopotamiense" (Mioceno Tardio-Plioceno Temprano) de la provincia de Entre Rios, Argentina. *Ameghiniana* 25:39-45.

Cozzuol MA. 1996. The records of the aquatic mammals in Southern South America. *Munchner Geowissenschaftliche Abhandlungen* 30:321-342.

Cozzuol MA. 2010. Fossil record and the evolutionary history of Inioidea. In: Ruiz-Garcia M, Shostell JM, eds. *Biology, Evolution and Conservation of River Dolphins within South America and Asia*. Hauppage: Nova Science Publishers:193-221.

Debey LB, Pyenson ND. 2013. Osteological correlates and phylogenetic analysis of deep diving in living and extinct pinnipeds: What good are big eyes? *Marine Mammal Science* 29:48-83.

De Gracia C, Carrillo-Briceño J, Schwarzhans W, Jaramillo C. 2012. An exceptional marine fossil fish assemblage reveals a highly productive deep-water environment in the Central American Seaway during the late Miocene. *Geological Society of America Abstracts with Programs* 44:164.

Fierstine HL. 1978. A new marlin, *Makaira panamensis* from the Late Miocene of Panama. *Copeia* 1978:1-11.

Flower WH. 1867. Description of the skeleton of *Inia geoffrensis* and of the skull of *Pontoporia blainvillii*, with remarks on the systematic position on these animals in the order Cetacea. *Transactions of the Zoological Society of London* 6: 87–116.

Fordyce RE. 2002. *Simocetus rayi* (Odontoceti: Simocetidae, New Family): a bizarre new archaic Oligocene dolphin from the eastern North Pacific. *Smithsonian Contributions to Paleobiology* 93:185-222.

Fordyce RE. 2009. Cetacean fossil record. In: Perrin WF, Würsig B, Thewissen, JGM, eds. *Encyclopedia of Marine Mammals*, second edition. Amsterdam: Elsevier, 207-215.

Fraser FC, Purves PE. 1960. Hearing in cetaceans. Evolution of the accessory air sacs and the structure and function of the outer and middle ear in recent cetaceans. *Bulletin of the British Museum of Natural History, Zoology* 7:1-140.

Geisler JH, Sanders AE. 2003. Morphological evidence for the phylogeny of Cetacea. *Journal of Mammalian Evolution* 10:23-129.

Geisler JH, McGowen MR, Yang G, Gatesy J. 2011. A supermatrix analysis of genomic, morphological, and paleontological data from crown Cetacea. *BMC Evolutionary Biology* 11:112.

Geisler JH, Godfrey SJ, Lambert O. 2012. A new genus and species of late Miocene inioid (Cetacea, Odontoceti) from the Meherrin River, North Carolina, U.S.A. *Journal of Vertebrate Paleontology* 32:198-211.

Gibson ML, Geisler JH. 2009. A new Pliocene dolphin (Cetacea: Pontoporiidae), from the Lee Creek Mine, North Carolina. *Journal of Vertebrate Paleontology* 29:966-971.

Godfrey SJ, Barnes LG. 2008. A new genus and species of late Miocene pontoporiid dolphin (Cetacea: Odontoceti) from the St. Marys Formation in Maryland. *Journal of Vertebrate Paleontology* 28:520-528.

Gowans S, Würsig B., & Karczmarski, L. (2007). The social structure and strategies of delphinids: predictions based on an ecological framework.*Advances in Marine Biology*, *53*, 195-294.

Gray JE. 1846. On the cetaceous animals. In: Richardson J, Gray JE, eds, *The Zoology of the Voyage of* H. M. S. Erebus *and* Terror*, under the Command of Capt. Sir J. C. Ross, R. N., F. R. S., During the Years 1839 to 1843*. London: E. W. Janson, 13–53.

Gingerich PD. 2005. Cetacea. In: Rose KD, Archibald JD, eds. *Placental mammals: origin, timing, and relationships of the major extant clades*. Baltimore: Johns Hopkins University Press, 234-252.

Gutstein CS, Cozzuol MA, Vargas AO, Suárez M, Schultz CL. 2009. Patterns of skull variation of *Brachydelphis* (Cetacea, Odontoceti, Pontoporiidae) from South-Easthern Pacific Neogene. *Journal of Mammalogy* 90:504-519.

Gutstein CS, Figueroa-Bravo CP, Pyenson ND, Yury-Yañez RE, Cozzuol MA, Canals M. 2014a. High frequency echolocation, ear morphology, and the marine–freshwater transition: A comparative study of extant and extinct toothed whales. *Palaeogeography, Palaeoclimatology, Palaeoecology* 400:62-74.

Gutstein CS, Cozzuol MA, Pyenson ND. 2014b. The antiquity of riverine adaptations in Iniidae (Cetacea, Odontoceti) documented by a humerus from the late Miocene of the Ituzaingó Formation, Argentina. *The Anatomical Record* 297:1096-1102.

Hamilton H, Caballero S, Collins AG, Brownell RL. 2001. Evolution of river dolphins. *Proceedings of the Royal Society of London B: Biological Sciences* 268:549-556.

Hendy AJW, Jones D, De Gracia D, Velez-Juarbe J. In press. Paleoecology of the Chagres Formation (latest Miocene) of Panama: reinterpreting the paleoenvironment of a vertebrate-rich marine fauna. *Journal of Geology*.

Hoorn C, Wesselingh FP, Steege H, Bermudez MA, Mora A, Sevink J, Sanmartín I, Sanchez-Meseguer A, Anderson CL, Figueiredo JP, Jaramillo J, Riff D, Negri FR, Hooghiemstra H, Lundberg J, Stadler T, Särkinen T, Antonelli A. 2010. Amazonia through time: Andean uplift, climate change, landscape evolution, and biodiversity. *Science* 330:927-931.

Jackson JBC, O'Dea A. 2013. Timing of the oceanographic and biological isolation of the Caribbean sea from the tropical eastern Pacific Ocean. *Bulletin of Marine Science* 89: 779-800.

Kelley NP, Pyenson ND. 2015. Evolutionary innovation and ecology in marine tetrapods from the Triassic to the Anthropocene. *Science* 348:aaa3716.

Lambert O, Post, K. 2005. First European pontoporiid dolphins (Mammalia: Cetacea, Odontoceti) from the Miocene of Belgium and The Netherlands. *Deinsea* 11:7-20.

Lambert O, de Muizon C. 2013. A new long-snouted species of the Miocene pontoporiid dolphin *Brachydelphis* and a review of the Mio-Pliocene marine mammal levels in the Sacaco Basin, Peru. *Journal of Vertebrate Paleontology* 33:709-721.

Leigh EG, O'Dea A, Vermeij GJ. 2014. Historical Biogeography of the Isthmus of Panama. *Biological Reviews* 89:148-72.

Lovejoy NR, Bermingham E, Martin AP. 1998. Marine incursion into South America. *Nature* 396: 421–422.

May-Collado, L. J. and I. Agnarsson. 2006. Cytochrome b and Bayesian inference of whale phylogeny. *Molecular Phylogenetics and Evolution* 38:344-354.

Mead JG, Fordyce RE. 2009. The therian skull: a lexicon with emphasis on the odontocetes. *Smithsonian Contributions to Zoology* 627:1-248.

Messenger SL, McGuire JA. 1998. Morphology, molecules, and the phylogenetics of cetaceans. Syst Biol 47:90-124.

Miller KG, Kominz MA, Browning JV, Wright JD, Mountain GS, Katz ME, Sugarman PJ, Cramer BS, Christie-Blick N, Pekar SF. 2005. The Phanerozoic record of global sea-level change. *Science* 310: 1293–1298.

Montes C, Cardona A, Jaramillo C, Pardo A, Silva JC, Valencia V, Ayala C, Pérez-Angel LC, Rodriguez-Parra LA, Ramirez V, Niño H. 2015. Middle Miocene closure of the Central American Seaway. *Science* 348: 226-229.

Morgan GS. 1994. Miocene and Pliocene marine mammal faunas from the Bone Valley Formation of Central Florida. In Berta A, Deméré TA, eds. *Contributions in Marine Mammal Paleontology Honoring Frank C. Whitmore, Jr.* Proceedings of the San Diego Society of Natural History 29:239–268.

Muizon C de. 1984. Les vertébré fossiles de la Formation Pisco (Pérou) Deuxiéme partie: les Odontocétes (Cetacea, Mammalia) du Pliocéne inerieur de Sud Sacaco. *Travaux de l'Institut Français d´Études Andines* 27:1-188.

Muizon C de. 1988a. Les relations phylogenétiques des Delphinida (Cetacea, Mammalia). *Annales de Paleontologie* 74:159-227.

Muizon C de. 1988b. Vertebrés fossiles de la Formation Pisco (Pérou) Troisiéme partie: Les Odontocètes (Cetacea: Mammalia) du Miocène. *Travaux de l'Institut Français d'Études Andines* 42: 1-244.

Murakami M, Shimada C, Hikida Y, Soeda Y, Hirano H. 2014. *Eodelphis kabatensis*, a new name for the oldest true dolphin *Stenella kabatensis* Horikawa, 1977 (Cetacea, Odontoceti, Delphinidae), from the upper Miocene of Japan, and the phylogeny and paleobiogeography of Delphinoidea. *Journal of Vertebrate Paleontology* 34:491-511.

Nikaido M, Matsuno F, Hamilton H, Brownell RL Jr, Cao Y, Ding W, Zuoyan Z, Shedlock AM, Fordyce RE, Hasegawa M, Okada N. 2001. Retroposon analysis of major cetacean lineages: the monophyly of toothed whales and the paraphyly of river dolphins. *Proceedings of the National Academy of Sciences* 1998:7384-7389.

O'Dea A, Jackson JB, Fortunato H, Smith JT, D'Croz L, Johnson KG, Todd JA. 2007. Environmental change preceded Caribbean extinction by 2 million years. *Proceedings of the National Academy of Sciences* 104:5501-5506.

O'Dea A, Jackson J. 2009. Environmental change drove macroevolution in cupuladriid bryozoans. *Proceedings of the Royal Society B: Biological Sciences* 276:3629-3634.

O'Dea A, Hoyos N, Rodríguez F, Degracia B, De Gracia C. 2012. History of upwelling in the Tropical Eastern Pacific and the paleogeography of the Isthmus of Panama. *Palaeogeography, Palaeoclimatology, Palaeoecology* 348:59-66.

Perrin, WF. 1975. Variation of spotted and spinner porpoise (genus Stenella) in the eastern Pacific and Hawaii. *Bulletin of the Scripps Institution of Oceanography of the University of California* 21:1–206.

Pyenson ND, Hoch E. 2007. Tortonian pontoporiid odontocetes from the eastern North Sea. *Journal of Vertebrate Paleontology* 27:757–762.

Pyenson ND. 2009. Requiem for *Lipotes*: An evolutionary perspective on marine mammal extinction. *Marine Mammal Science* 25:714-724.

Pyenson ND, Sponberg SN. 2011. Reconstructing body size in extinct crown Cetacea (Neoceti) using allometry, phylogenetic methods and tests from the fossil record. *Journal of Mammalian Evolution* 18:269-288.

Pyenson ND, Kelley NP, Parham JF. 2014a. Marine tetrapod macroevolution: Physical and biological drivers on 250Ma of invasions and evolution in ocean ecosystems. *Palaeogeography, Palaeoclimatology, Palaeoecology* 400: 1-8.

Pyenson ND, Gutstein CS, Parham JF, Le Roux JP, Chavarría CC, Little H, Metallo A, Rossi V, Valenzuela-Toro AM, Velez-Juarbe J, Santelli CM, Rubilar Rogers D, Cozzuol MA, Suárez, M. E. 2014. Repeated mass strandings of Miocene marine mammals from Atacama Region of Chile point to sudden death at sea. *Proceedings of the Royal Society B: Biological Sciences* 281:20133316.

Reinhart RH. 1959. A review of the Sirenia and Desmostylia. *University of California Publications in Geological Sciences* 36:1-146

Rensberger JM. 1969. A new iniid cetacean from the Miocene of California. *University of California Publications in Geological Sciences* 82:1-34.

Ruiz-Garcia M, Shostell JM. 2010. Biology, Evolution and Conservation of River Dolphins within South America and Asia. Hauppauge: Nova Science Publishers: 1-504.

Robbins JA, Tao J, Grossman EL, O'Dea A. 2012. Exploring the delayed overturn in Caribbean fauna using gastropod stable-isotope profiles to quantify seasonal upwelling and freshening of coastal waters. *Geological Society of America Abstracts with Programs* 44.

Scapino R. 1981. Morphological investigation into functions of the jaw symphysis in carnivorans. *Journal of Morphology* 167:339–375.

Schusterman RJ, Kastak D, Levenson DH, Reichmuth CJ, Southall BL. 2000. Why pinnipeds don't echolocate. *The Journal of the Acoustical Society of America* 107:2256-2264.

Schwarzhans W, Aguilera O. 2013. Otoliths of the Myctophidae from the Neogene of tropical America. *Palaeo Ichthyologica* 13:83-150.

Simpson GG. 1945. The principles of classification, and a classification of mammals. *Bulletin of the American Museum of Natural History* 85:1-350.

Steeman ME, Hebsgaard MB, Fordyce RE Ho, SYW, Rabosky DL, Nielsen R, Rahbek C, Glenner H, Sørensen MV, Willerslev E. 2009. Radiation of extant cetaceans driven by restructuring of the oceans. *Systematic Biology* 58:573-585.

Swofford DL. 2002. PAUP* v.40b10. Sinauer Associates, Sunderland.

Tanaka Y, Fordyce RE. 2014. Fossil dolphin *Otekaikea marplesi* (latest Oligocene, New Zealand) expands the morphological and taxonomic diversity of Oligocene cetaceans. *PLoS ONE* 9:e107972.

Thewissen JG, Williams EM. 2002. The early radiations of Cetacea (Mammalia): evolutionary pattern and developmental correlations. *Annual Review of Ecology and Systematics* 33:73-90.

Turvey ST, Barrett LA, Yujiang HAO, Lei Z, Xinqiao Z, Xianyan W, Yadong H, Kaiya Z, Hart T, Ding W. 2010. Rapidly shifting baselines in Yangtze fishing communities and local memory of extinct species. *Conservation Biology* 24:778-787.

Velez-Juarbe J, Wood AR, De Gracia C, Hendy AJW. In press. Evolutionary patterns among living and fossil kogiid sperm whales: evidence from the Neogene of Central America. *PLoS ONE*.

Vermeij GJ, Dudley R. 2000. Why are there so few evolutionary transitions between aquatic and terrestrial ecosystems? *Biological Journal of the Linnean Society* 70:541-554

Vigil DI, Laurito CA. 2014. New fossil remains of an odontoceti (mammalia: Cetacea, physeteroidea) from the late miocene of Panama, Central America. *Revista Geológica de América Central* 50:213-217.

Werth AJ. 2006. Mandibular and dental variation and the evolution of suction feeding in Odontoceti. *Journal of Mammalogy* 87:579-588.

Whitmore FC Jr. 1994. Neogene climate change and the emergence of the modern whale fauna of the North Atlantic Ocean. In Berta A, Deméré TA, eds. *Contributions in Marine Mammal Paleontology Honoring Frank C. Whitmore, Jr.* Proceedings of the San Diego Society of Natural History 29:223–228.

TABLE CAPTIONS

Table 1. Measurements of holotype skull and mandibles (USNM 546125) of [redacted] gen. nov., sp. nov., in mm (modified after Perrin, 1975 and Tanaka and Fordyce, 2014). Asterisk indicates doubling of measurement from one side. Positive sign indicates preserved distance.

Table 2. Measurements of the scapula (USNM 546125) of [redacted] gen. nov., sp. nov., in mm (modified after Perrin, 1975).

Table 3. Relative orbit size (ROS) in [redacted] and in other fossil and modern odontocetes, ranked in increasing value.

Table 1.

Skull	Measurement (mm)
Total length from the most anterior point to the posterior most point	571+
Cranial length	185+
Length of rostrum—from tip to line across hindmost limits of antorbital notches:	381
Width of rostrum at base—along line across hindmost limits of antorbital notches:	124*
Width of rostrum at 60 mm anterior to line across hindmost limits of antorbital notches:	90*
Width of rostrum at midlength:	36+
Width of premaxillae at midlength of rostrum:	31+
Width of rostrum at 3/4 length, measured from posterior end:	50*
Greatest width of premaxillae:	78*
Projection of premaxillae beyond maxillae measured from tip of rostrum to line across foremost tips of maxillae visible in dorsal view:	85+
Width of premaxillae at a line across posterior limits of anorbital notces	48*
Maximum width of premaxillae at mid-orbit level	52*
Preorbital width at level of frontal-lacrimal suture	184*
Postorbital width across apices of postorbital processes	232*
Distance from tip of rostrum to external nares (to mesial end of anterior transverse margin of right naris):	419+
Distance from foremost end of junction between nasals to hindmost point of margin of supraoccipital crest:	68
Greatest width of external nares:	49
Median length of the nasals:	58
Maximum length of the right nasal:	58
Median length of frontals on the vertex:	25
Vertical external height of the skull from ventral most braincase to dorsal extremity of vertex:	150+
Bizygomatic width	262*
Length of upper left tooth row—from hindmost margin of hindmost alveolus to tip of rostrum:	329
Number of teeth—upper left:	18
Number of teeth—upper right:	18
Mandible	
Maximum preserved length of left mandible	478+
Maximum preserved height of left mandible	74+
Number of teeth—lower left:	18
Number of teeth—lower right:	18
Length of the lower tooth row from tip of mandible to posterior margin of posterior most alveolus:	315

Table 2.

Scapula	Measurement (mm)
Maximum height of scapula	**141+**
Height of scapula from posterior margin of glenoid fossa to glenovertebral angle	161
Length of coracoid process	40
Greatest width of coracoid process	23
Greatest width of acromion process	26

Table 3

Genus	species	Specimen	ROS	Source
Aulophyseter	*morricei*	LACM 154100, USNM 11230	0.20	This study (average, n = 2)
Orycterocetus	*crocodilinus*	USNM 22926	0.22	This study
Inia	*geoffrensis*	USNM 23967, 49582, 395415	0.24	This study (average, n = 3)
Lipotes	*vexillifer*	USNM 218293	0.32	This study
Aprixokogia	*kelloggi*	USNM 187015	0.34	This study
Lophocetus	*repenningi*	USNM 23886	0.36	This study
Simocetus	*rayi*	USNM 356517	0.36	This study
[redacted]	[redacted]	**USNM 546125**	**0.40**	**This study**
Nanokogia	*isthmia*	UF 280000	0.40	Velez-Juarbe et al., in press
Xiphiacetus	*bossi*	USNM 8842, 175381	0.42	This study (average, n = 2)
Delphinodon	*dividum*	USNM 7278	0.46	This study
Kogia	*sima*	LACM 47142	0.55	This study
Meherrinia	*isoni*	IRSNB M.2013	0.56	Geisler et al., 2012
Pontoporia	*blainvillei*	USNM 482707, 482717, 482771	0.57	This study (average, n = 3)
Atocetus	*nasalis*	LACM 30093	0.58	Barnes, 1985b
Kentriodon	*pernix*	USNM 8060	0.58	This study
Parapontoporia	*wilsoni*	UCMP 83790	0.62	Barnes, 1985a
Brachydelphis	*jahuayensis*	PPI 267, 268; MUSM 567, 568	0.70	Lambert & Muizon, 2013 (average, n = 4)
Brachydelphis	*mazeasi*	PPI 121, 266; MUSM 564	0.80	Lambert & Muizon, 2013 (average, n = 3)

FIGURES CAPTIONS

Figure 1. Geographic and stratigraphic context of [redacted] A) Map of Central America with a yellow star representing the type locality, STRI locality 650009. B) Map of north-central Panama with the distribution of the Chagres Formation, with type locality of [redacted] in the vicinity of Piña, along with other fossil vertebrates. C) Chronostratigraphic and lithostratigraphic relationships of the Chagres Formation. (Modified from Hendy et al., in press, and Velez-Juarbe et al., in press).

Figure 2. Collecting the type specimen of [redacted] at the type locality on 18 June 2011. A) The specimen exposed in the outcrop, at low tide, with the scapula, oriented lateral side facing stratigraphic up, approximately 35 cm away from the skull, which was exposed ventral side up. Scale bar = 10 cm. Photo: J. Velez-Juarbe. B) With the high tide returning, removal of the plaster jacketed sediment block, containing the skull, exposed the mandibles located directly underneath it. The mandible was oriented dorsal surface facing stratigraphic up. Photo: A. O'Dea.

Figure 3. Dorsal views of the type skull of [redacted] (USNM 546125) from A) photographs and B) orthogonal digital three-dimensional polygon model prepared from CT data, with lighting and color modifications using the Smithsonian X 3D browser. See <link> to measure, modify, or download this model. C) Anterior and D) posterior views of the type skull of [redacted] (USNM 546125) from orthogonal digital three-dimensional polygon model prepared from CT data, with lighting and color modifications using the Smithsonian X 3D browser. See http://3d.si.edu/explorer?s=h2mqJ9 (dorsal view), http://3d.si.edu/explorer?s=bA5gJO (posterior view), and http://3d.si.edu/explorer?s=e1seD5 (anterior view) to measure, modify, or download this model. Abbreviations: alis, alisphenoid; gf, glenoid fossa; fr, frontal; ju, jugal; la, lacrimal; max, maxilla; mc, maxillary crest; me, mesthmoid; na,

nasal; nar, naris; nuc, nuchal crest; pa, parietal; pdif, posterior dorsal infraorbital foramen; pmax, premaxilla; pmaxf, premaxillary foramen; popf, posterior process of the postorbital process of the frontal; smf, sternomastoid fossa; socc, supraoccipital; sq, squamosal; zpsq, zygomatic process of the squamosal.

Figure 4. Ventral views of the type skull of [redacted] (USNM 546125) from A) photographs and B) orthogonal digital three-dimensional polygon model prepared from CT data, with lighting and color modifications using the Smithsonian X 3D browser. See http://3d.si.edu/explorer?s=iEpExr to measure, modify, or download this model. Abbreviations: alis, alisphenoid; ant, anterior; ext nar, external bony naris; I, incisor teeth; C, canine tooth; ju, jugal; la, lacrimal; max, maxilla; pa, parietal; PC, postcanine teeth; pmax, premaxilla; propf, preorbital process of the postorbital process of the frontal; popf, posterior process of the postorbital process of the frontal; smf, sternomastoid fossa; socc, supraoccipital; sq, squamosal; vom, vomer.

Figure 5. Right lateral views of the type skull of [redacted] (USNM 546125) from A) photographs and B) orthogonal digital three-dimensional polygon model prepared from CT data, with lighting and color modifications using the Smithsonian X 3D browser. See http://3d.si.edu/explorer?s=jn4ynp to measure, modify, or download this model. Abbreviations: alis, alisphenoid; fr, frontal; I, incisor teeth; C, canine tooth; ju, jugal; la, lacrimal; na, nasal; max, maxilla; pa, parietal; PC, postcanine teeth; pmax, premaxilla; propf, preorbital process of the postorbital process of the frontal; popf, posterior process of the postorbital process of the frontal; smf, sternomastoid fossa; socc, supraoccipital; sq, squamosal; zpsq, zygomatic process of the squamosal.

.

Figure 6. Computed tomography (CT) slices through the vertex of [redacted] (USNM 546125) across four slightly sub-transverse planes that pass anterior to posterior, A-D. Numbers 1 and 2 denote facial and endocranial sagittal midlines, respectively, showing the sinistral displacement of the facial bones (Geisler & Sanders, 2003; Mead & Fordyce, 2009). Abbreviations: alis, alisphenoid; fr, frontal; na, nasal; max, maxilla; pdif, posterior dorsal infraorbital foramen; socc, supraoccipital; sq, squamosal; tc, temporal crest; zpsq, zygomatic process of the squamosal.

Figure 7. Dorsal views of the mandibles of [redacted] (USNM 546125) from A) photographs and B) orthogonal digital three-dimensional polygon model prepared from CT data, with lighting and color modifications using the Smithsonian X 3D browser. C) Anterior and D) posterior views of the mandibles of [redacted] (USNM 546125) from orthogonal digital three-dimensional polygon model prepared from CT data, with lighting and color modifications using the Smithsonian X 3D browser. See http://3d.si.edu/explorer?s=hhl3iu (dorsal view), http://3d.si.edu/explorer?s=cgvhM3 (posterior view), and http://3d.si.edu/explorer?s=gR4Rhv (anterior view) to measure, modify, or download this model. Abbreviations: ap, angular process; (cp); coronoid process, parentheses denote this structure is not preserved; mef, mental foramina; mf, mandibular foramen; ms, mandibular symphysis.

Figure 8. Ventral views of the mandibles of [redacted] (USNM 546125) from A) photographs and B) orthogonal digital three-dimensional polygon model prepared from CT data, with lighting and color modifications using the Smithsonian X 3D browser. C) Left lateral and D) right lateral views of the mandibles of [redacted] (USNM 546125) from orthogonal digital three-dimensional polygon model prepared from CT data, with lighting and color modifications using the Smithsonian X 3D browser. See http://3d.si.edu/explorer?s=cavfn3 (ventral view),

http://3d.si.edu/explorer?s=dGTRVj (left lateral), and http://3d.si.edu/explorer?s=cLO5aZ (right lateral) to measure, modify, or download this model. Abbreviations: ap, angular process; (cp); coronoid process, parentheses denote this structure is not preserved; mef, mental foramina; mf, mandibular foramen; ms, mandibular symphysis.

Figure 9. A) Lateral, B) medial, and C) distal views of the type scapula of [redacted] (USNM 546125) and isolated teeth collected near the skull at the outcrop surface, showing D, upper left posterior tooth, E), lower left tooth posterior (almost certainly PC_{12}), and F), upper left posterior tooth (likely PC^3). Abbreviations: gf, glenoid fossa.

Figure 10. Phylogenetic analysis of [redacted] and other inioid odontocetes, showing a strict consensus tree resulting from six most parsimonious trees, 95 steps long, with CI = 0.283 and RI = 0.451. Numbers below nodes indicate decay index/bootstrap values; stem-based clades are indicated by arcs, while open circles denote node-based clades.

Figure 11. Life reconstruction of [redacted] by J. Molnar, feeding on a flatfish, which would have been abundant in the neritic zone of the late Miocene equatorial seas of Panama.

Figure 12. Time calibrated phylogenetic tree of select Delphinida, including [redacted] with Delphinoidea collapsed. Stratigraphic range data derives from published accounts for each taxon, including global ranges. Geologic time scale based on Cohen et al. (2013). Calibration for nodes follow mean divergence date estimates by McGowen et al. (2009:table 3) for the following clades: a, Delphinida (24.75 Ma); b, Inioidea+*Lipotes* (22.15 Ma); c, Delphinoidea (18.66 Ma); and Inioidea (in open white circle, 16.68 Ma). Arc indicates stem-based clade, Pan-Iniidae. Ecological habitat

preference is based on depositional environment or extant habitat. Abbreviations: Aquitan., Aquitanian; H., Holocene; Langh., Langhian; Ma, millions of years ago; Mess., Messinian; P., Piacenzian; Ple., Pleistocene; Plioc., Pliocene; Serra., Serravallian; Zan., Zanclean.

1

Figure 1

Figure 1. Geographic and stratigraphic context of [redacted] A) Map of Central America with a yellow star representing the type locality, STRI locality 650009. B) Map of north-central Panama with the distribution of the Chagres Formation, with type locality of [redacted] in the vicinity of Piña, along with other fossil vertebrates. C) Chronostratigraphic and lithostratigraphic relationships of the Chagres Formation. (Modified from Hendy et al., in press, and Velez-Juarbe et al., in press).

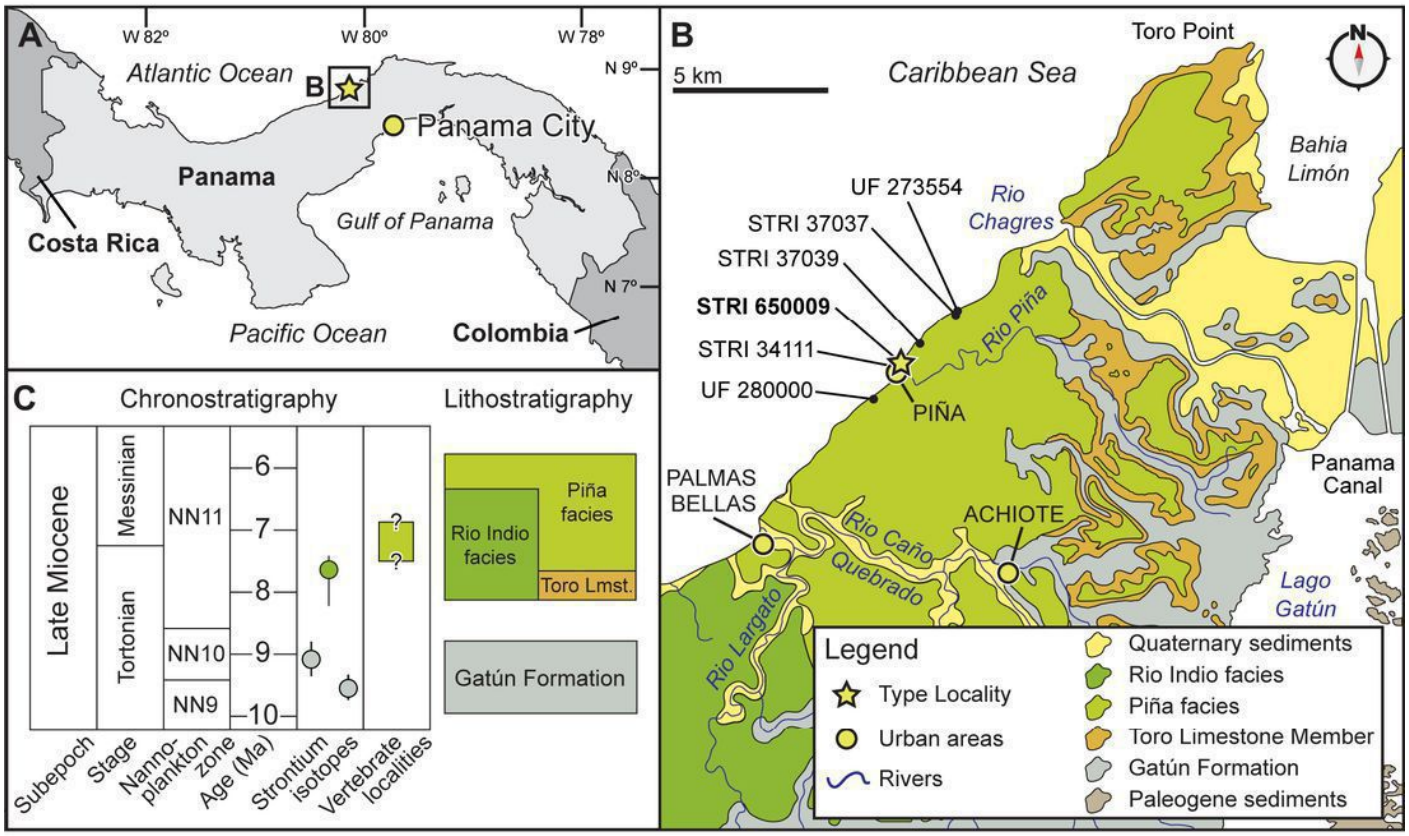

2

Figure 2

Figure 2. Collecting the type specimen of [redacted] at the type locality on 18 June 2011. A) The specimen exposed in the outcrop, at low tide, with the scapula, oriented lateral side facing stratigraphic up, approximately 35 cm away from the skull, which was exposed ventral side up. Scale bar = 10 cm. Photo: J. Velez-Juarbe. B) With the high tide returning, removal of the plaster jacketed sediment block, containing the skull, exposed the mandibles located directly underneath it. The mandible was oriented dorsal surface facing stratigraphic up. Photo: A. O'Dea.


A
N
scapula
cranium
rostrum
right naris
squamosal
B
skull block
mandibular
rami *in situ*

3

Figure 3

Figure 3. Dorsal views of the type skull of [redacted] (USNM 546125) from A) photographs and B) orthogonal digital three-dimensional polygon model prepared from CT data, with lighting and color modifications using the Smithsonian X 3D browser. See to measure, modify, or download this model. C) Anterior and D) posterior views of the type skull of [redacted] (USNM 546125) from orthogonal digital three-dimensional polygon model prepared from CT data, with lighting and color modifications using the Smithsonian X 3D browser. See http://3d.si.edu/explorer?s=h2mqJ9 (dorsal view), http://3d.si.edu/explorer?s=bA5gJO (posterior view), and http://3d.si.edu/explorer?s=e1seD5 (anterior view) to measure, modify, or download this model. Abbreviations: alis, alisphenoid; gf, glenoid fossa; fr, frontal; ju, jugal; la, lacrimal; max, maxilla; mc, maxillary crest; me, mesthmoid; na, nasal; nar, naris; nuc, nuchal crest; pa, parietal; pdif, posterior dorsal infraorbital foramen; pmax, premaxilla; pmaxf, premaxillary foramen; popf, posterior process of the postorbital process of the frontal; smf, sternomastoid fossa; socc, supraoccipital; sq, squamosal; zpsq, zygomatic process of the squamosal.

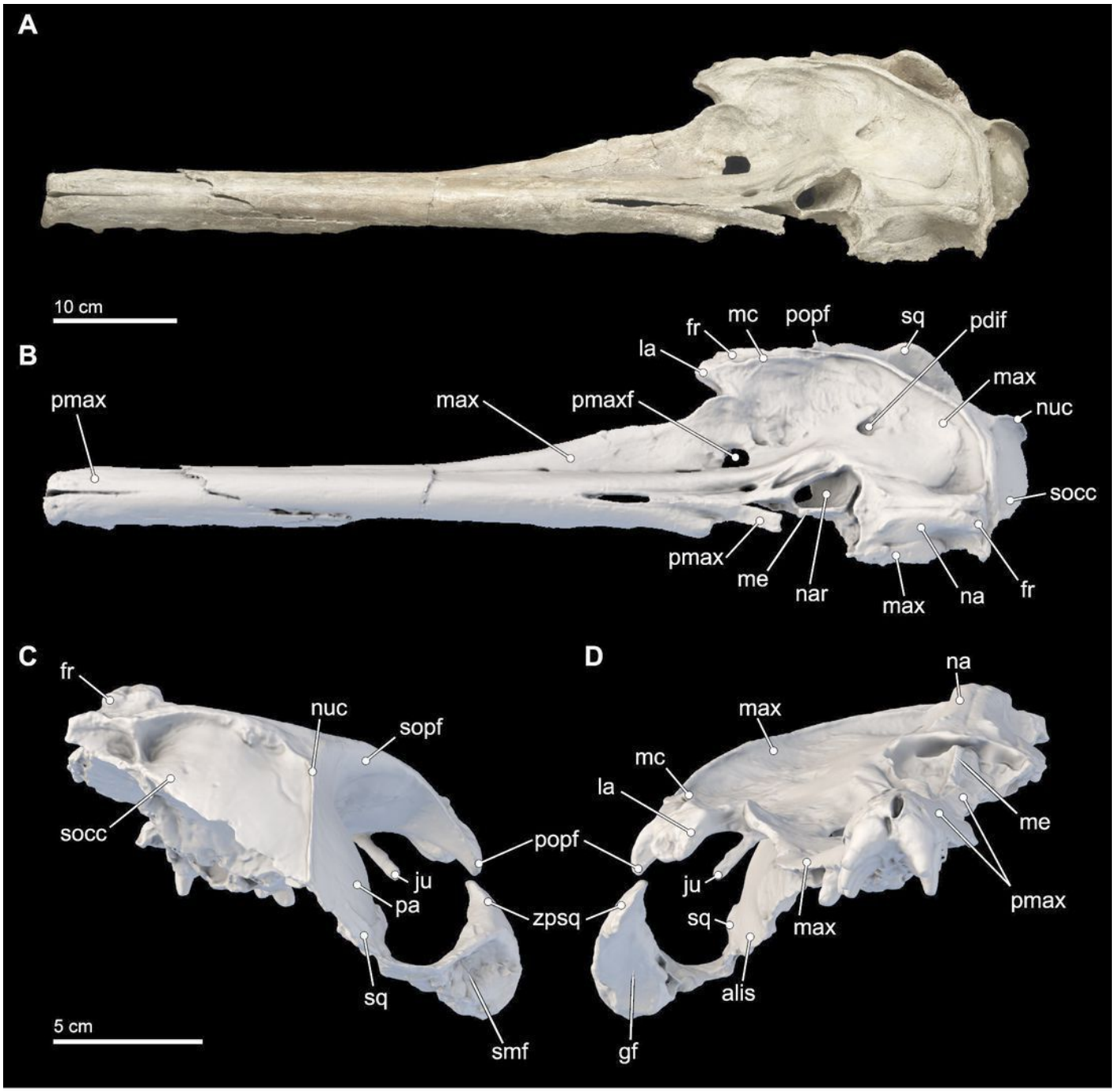
A
10 cm
B
pmax
max
pmaxf
fr
mc
popf
sq
pdif
la
max
nuc
socc
pmax
me
nar
max
na
fr
C
fr
nuc
sopf
socc
popf
ju
pa
zpsq
sq
smf
5 cm
D
na
max
mc
la
me
ju
pmax
sq
max
alis
gf

4

Figure 4

Figure 4. Ventral views of the type skull of [redacted] (USNM 546125) from A) photographs and B) orthogonal digital three-dimensional polygon model prepared from CT data, with lighting and color modifications using the Smithsonian X 3D browser. See http://3d.si.edu/explorer?s=iEpExr to measure, modify, or download this model. Abbreviations: alis, alisphenoid; ant, anterior; ext nar, external bony naris; I, incisor teeth; C, canine tooth; ju, jugal; la, lacrimal; max, maxilla; pa, parietal; PC, postcanine teeth; pmax, premaxilla; propf, preorbital process of the postorbital process of the frontal; popf, posterior process of the postorbital process of the frontal; smf, sternomastoid fossa; socc, supraoccipital; sq, squamosal; vom, vomer.

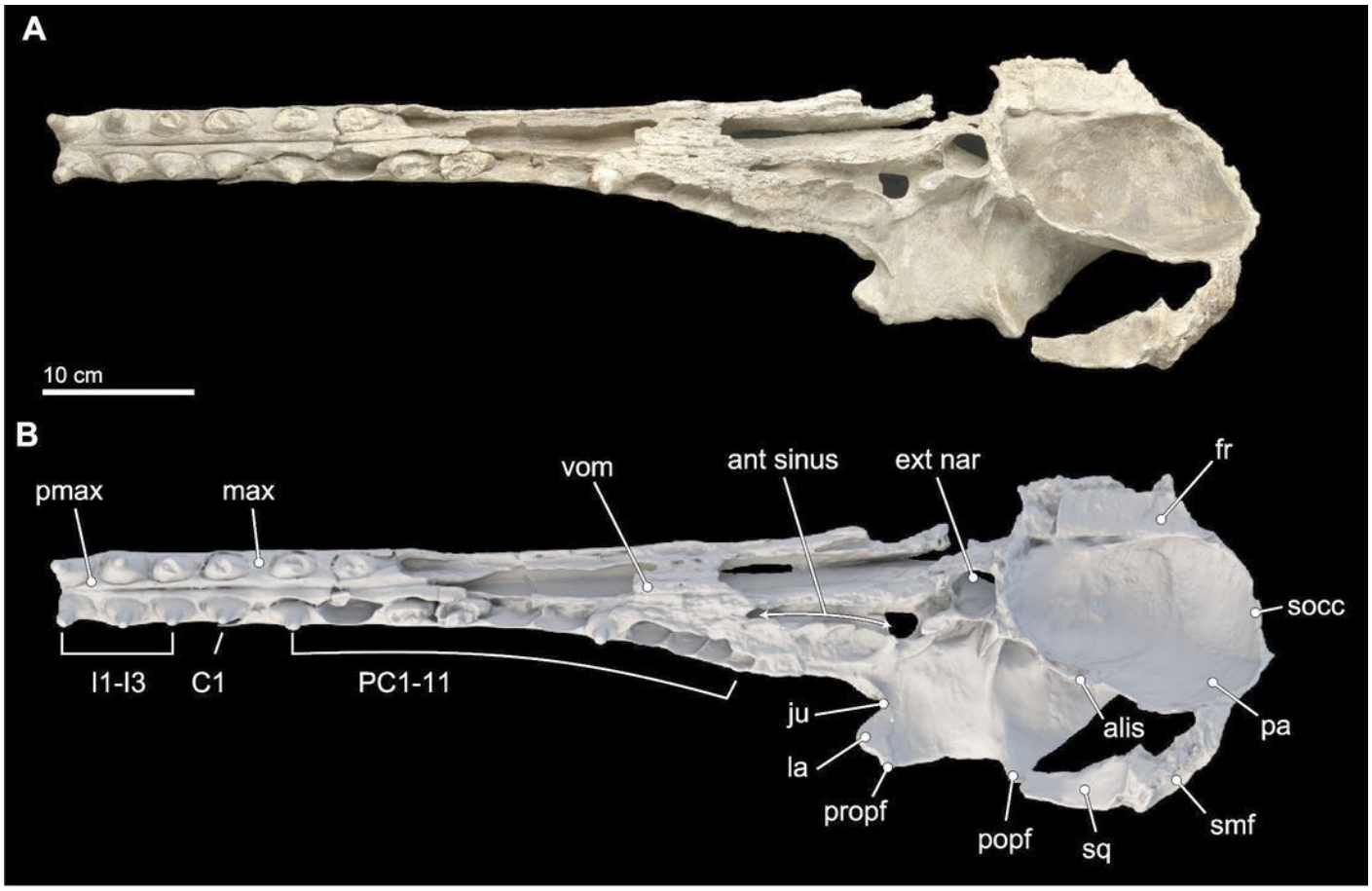

5

Figure 5

Figure 5. Right lateral views of the type skull of [redacted] (USNM 546125) from A) photographs and B) orthogonal digital three-dimensional polygon model prepared from CT data, with lighting and color modifications using the Smithsonian X 3D browser. See http://3d.si.edu/explorer?s=jn4ynp to measure, modify, or download this model. Abbreviations: alis, alisphenoid; fr, frontal; I, incisor teeth; C, canine tooth; ju, jugal; la, lacrimal; na, nasal; max, maxilla; pa, parietal; PC, postcanine teeth; pmax, premaxilla; propf, preorbital process of the postorbital process of the frontal; popf, posterior process of the postorbital process of the frontal; smf, sternomastoid fossa; socc, supraoccipital; sq, squamosal; zpsq, zygomatic process of the squamosal.

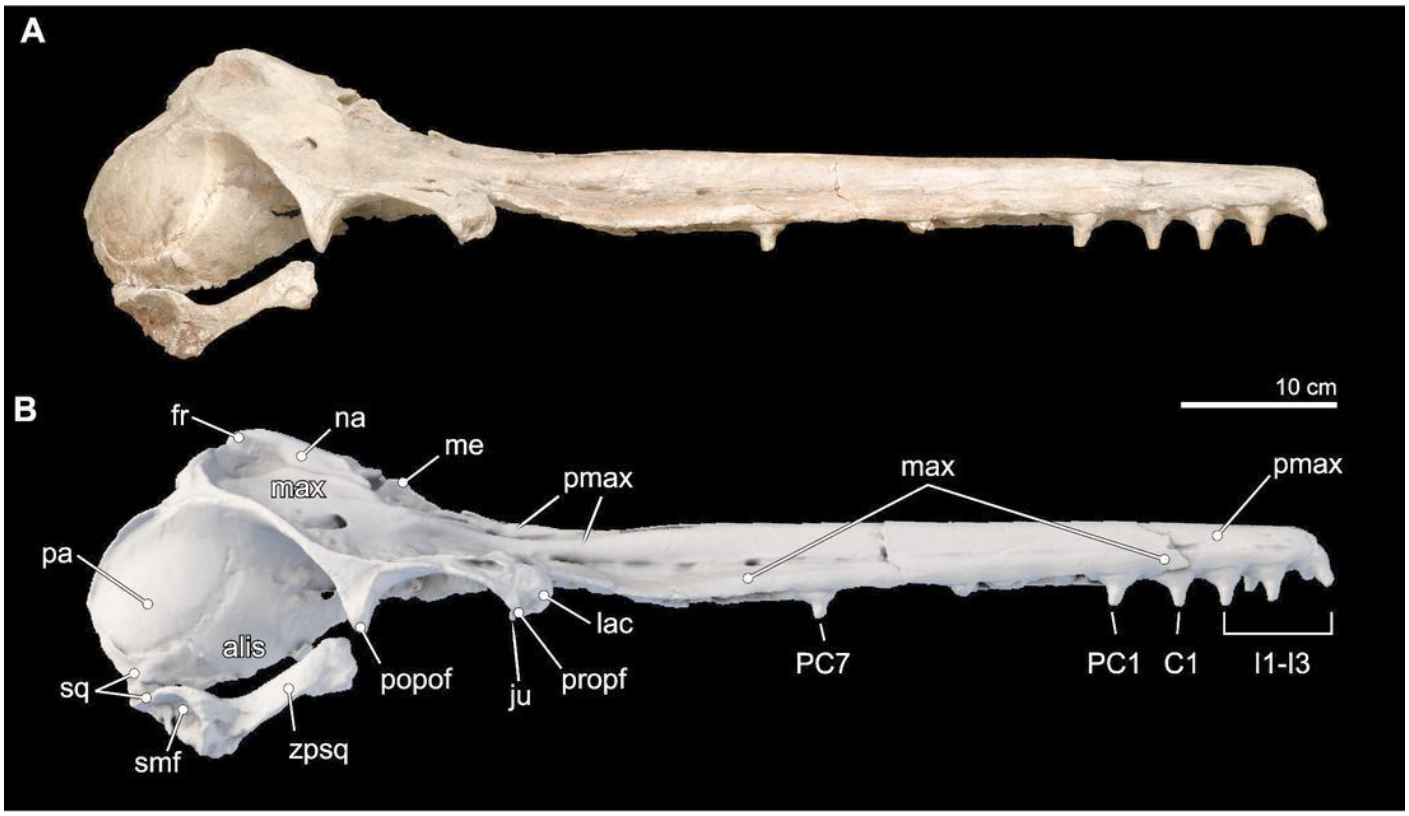

6

Figure 6

Figure 6. Computed tomography (CT) slices through the vertex of [redacted] (USNM 546125) across four slightly sub-transverse planes that pass anterior to posterior, A-D. Numbers 1 and 2 denote facial and endocranial sagittal midlines, respectively, showing the sinistral displacement of the facial bones (Geisler & Sanders, 2003; Mead & Fordyce, 2009). Abbreviations: alis, alisphenoid; fr, frontal; na, nasal; max, maxilla; pdif, posterior dorsal infraorbital foramen; socc, supraoccipital; sq, squamosal; tc, temporal crest; zpsq, zygomatic process of the squamosal.

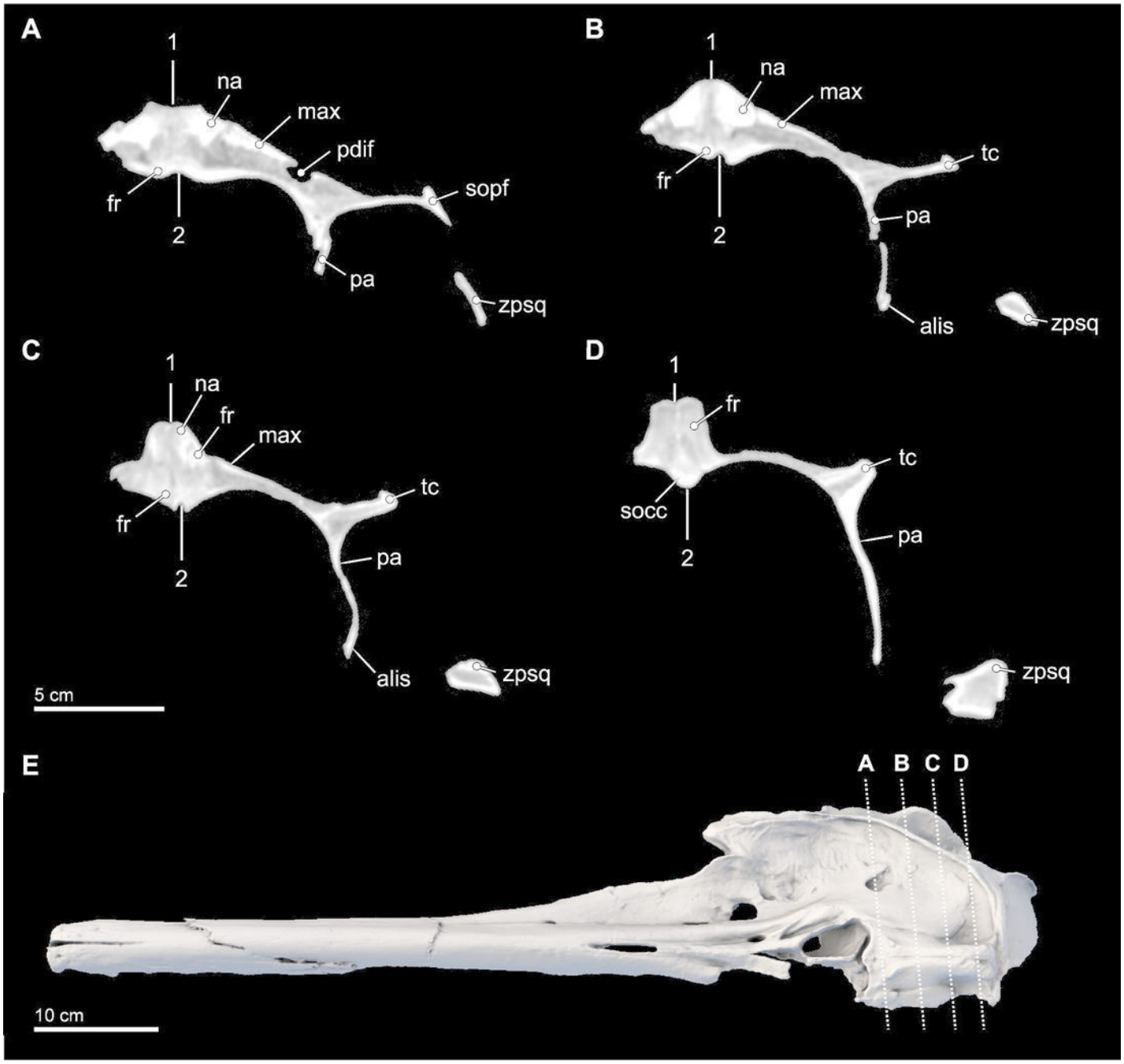
A
1
na
max
pdif
fr
2
sopf
pa
zpsq
B
1
na
max
tc
fr
2
pa
alis
zpsq
C
1
na
fr
max
tc
fr
2
pa
alis
zpsq
5 cm
D
1
fr
tc
socc
2
pa
zpsq
E
A B C D
10 cm

7

Figure 7

Figure 7. Dorsal views of the mandibles of [redacted] (USNM 546125) from A) photographs and B) orthogonal digital three-dimensional polygon model prepared from CT data, with lighting and color modifications using the Smithsonian X 3D browser. C) Anterior and D) posterior views of the mandibles of [redacted] (USNM 546125) from orthogonal digital three-dimensional polygon model prepared from CT data, with lighting and color modifications using the Smithsonian X 3D browser. See http://3d.si.edu/explorer?s=hhl3iu (dorsal view), http://3d.si.edu/explorer?s=cgvhM3 (posterior view), and http://3d.si.edu/explorer?s=gR4Rhv (anterior view) to measure, modify, or download this model. Abbreviations: ap, angular process; (cp); coronoid process, parentheses denote this structure is not preserved; mef, mental foramina; mf, mandibular foramen; ms, mandibular symphysis.

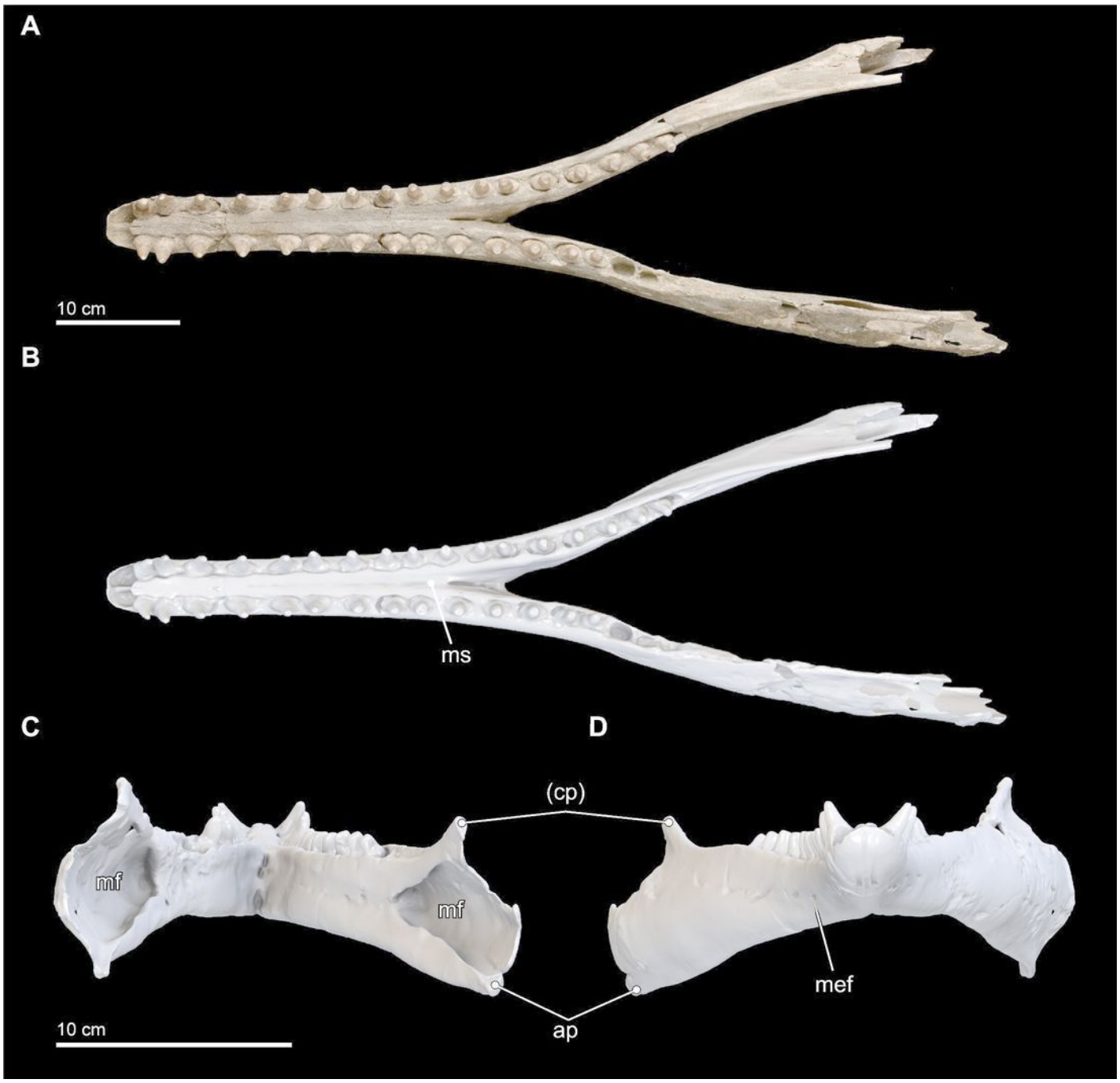
A
10 cm
B
ms
C
D
(cp)
mf
mf
mef
ap
10 cm

8

Figure 8

Figure 8. Ventral views of the mandibles of [redacted] (USNM 546125) from A) photographs and B) orthogonal digital three-dimensional polygon model prepared from CT data, with lighting and color modifications using the Smithsonian X 3D browser. C) Left lateral and D) right lateral views of the mandibles of [redacted] (USNM 546125) from orthogonal digital three-dimensional polygon model prepared from CT data, with lighting and color modifications using the Smithsonian X 3D browser. See http://3d.si.edu/explorer?s=cavfn3 (ventral view), http://3d.si.edu/explorer?s=dGTRVj (left lateral), and http://3d.si.edu/explorer?s=cLO5aZ (right lateral) to measure, modify, or download this model. Abbreviations: ap, angular process; (cp); coronoid process, parentheses denote this structure is not preserved; mef, mental foramina; mf, mandibular foramen; ms, mandibular symphysis.

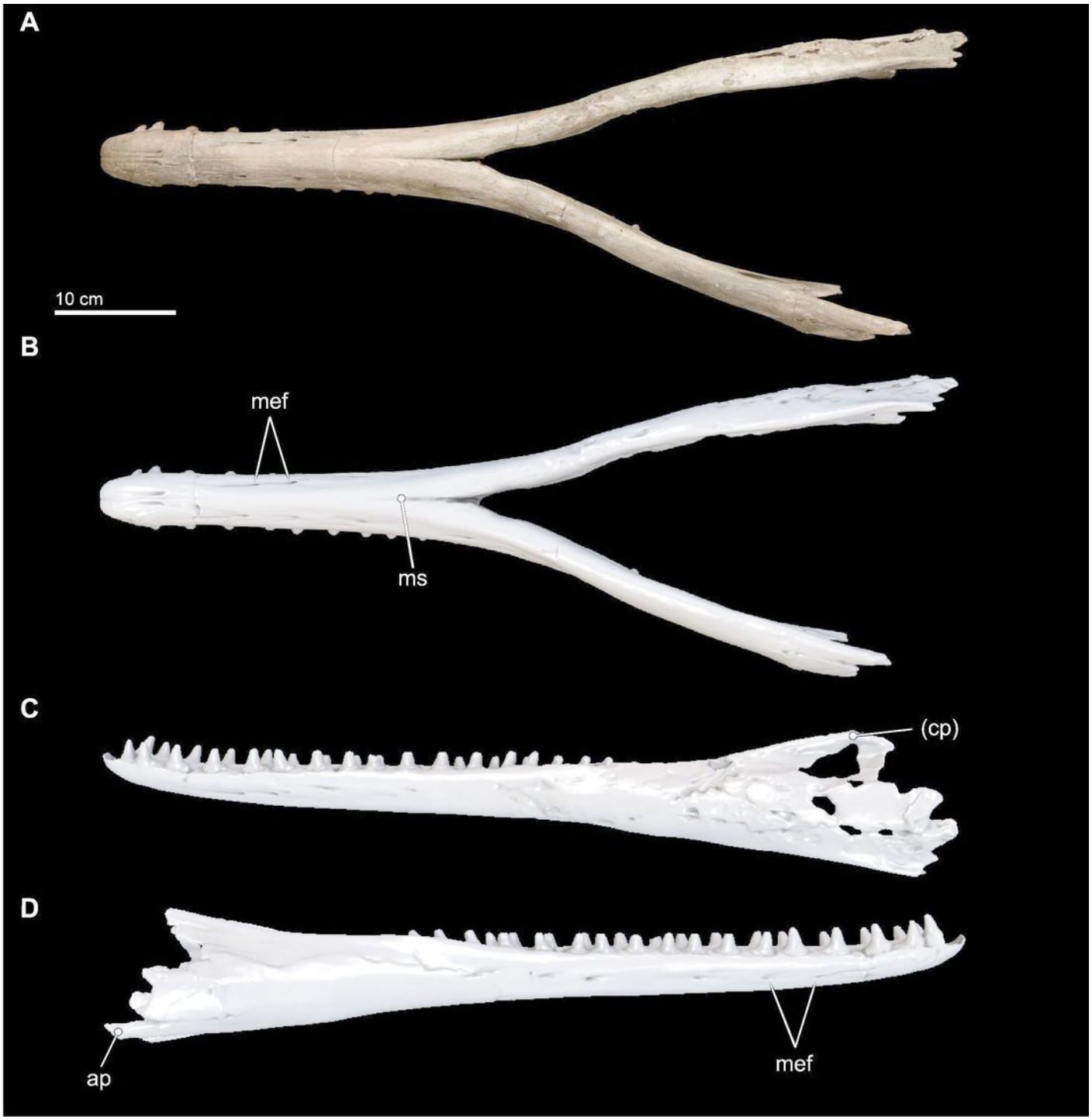
A
10 cm
B
mef
ms
C
(cp)
D
ap
mef

9

Figure 9

Figure 9. A) Lateral, B) medial, and C) distal views of the type scapula of [redacted] (USNM 546125) and isolated teeth collected near the skull at the outcrop surface, showing D, upper left posterior tooth, E), lower left tooth posterior (almost certainly PC12), and F), upper left posterior tooth (likely PC3). Abbreviations: gf, glenoid fossa.

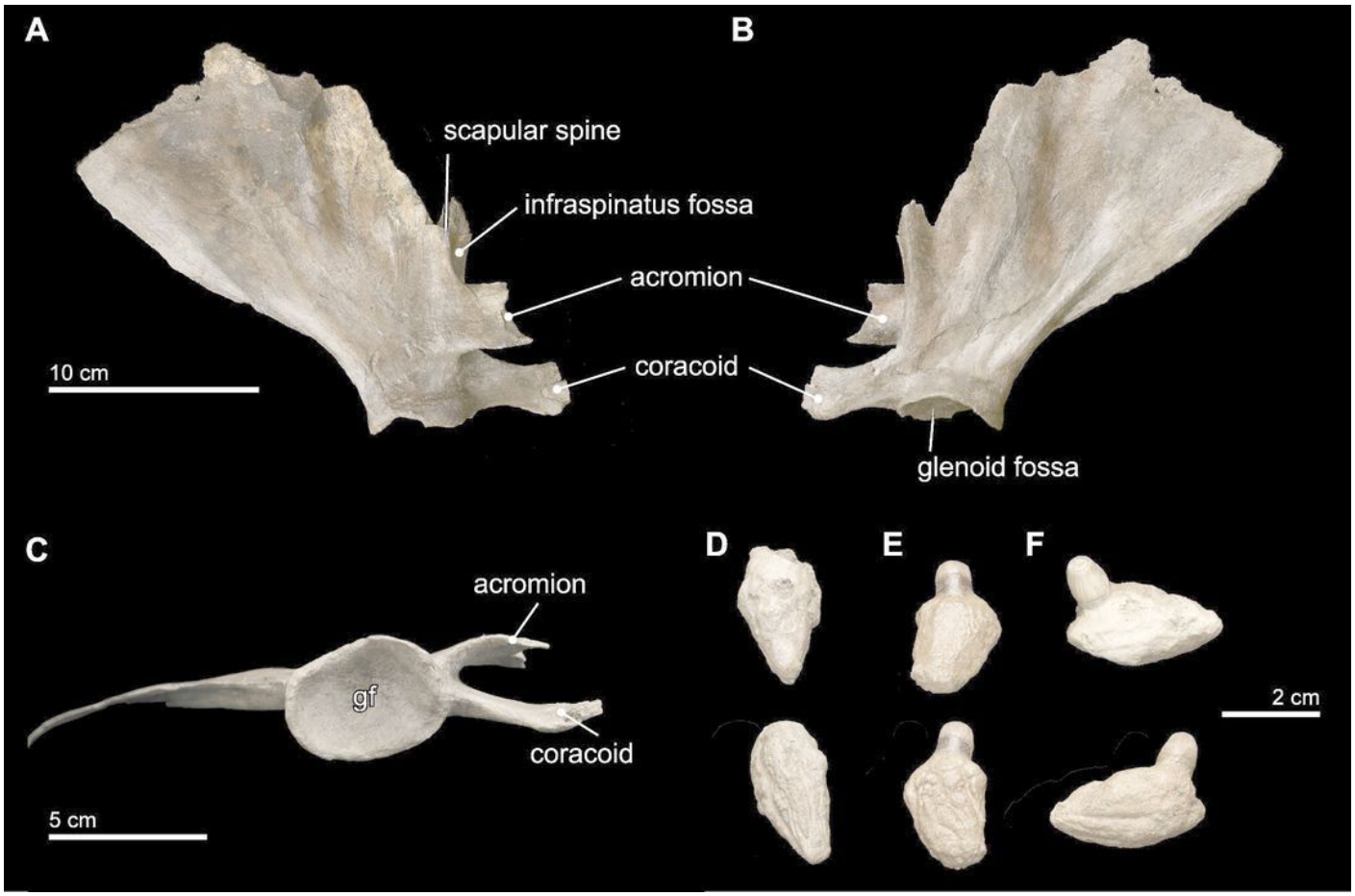

10

Figure 10

Figure 10. Phylogenetic analysis of [redacted] and other inioid odontocetes, showing a strict consensus tree resulting from six most parsimonious trees, 95 steps long, with CI = 0.283 and RI = 0.451. Numbers below nodes indicate decay index/bootstrap values; stem-based clades are indicated by arcs, while open circles denote node-based clades.

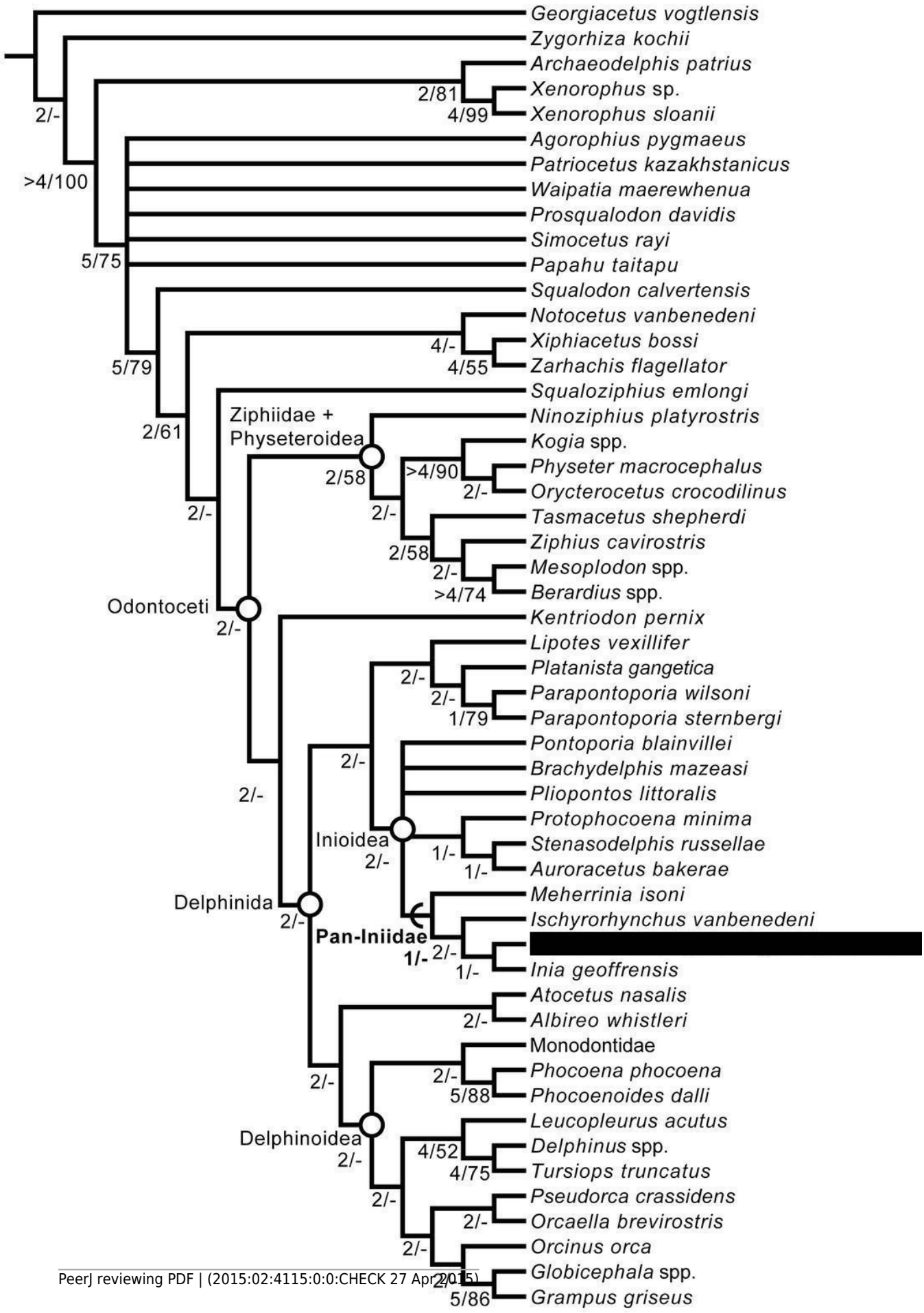
Georgiacetus vogtlensis
Zygorhiza kochii
Archaeodelphis patrius
Xenorophus sp.
Xenorophus sloanii
Agorophius pygmaeus
Patriocetus kazakhstanicus
Waipatia maerewhenua
Prosqualodon davidis
Simocetus rayi
Papahu taitapu
Squalodon calvertensis
Notocetus vanbenedeni
Xiphiacetus bossi
Zarhachis flagellator
Squaloziphius emlongi
Ninoziphius platyrostris
Kogia spp.
Physeter macrocephalus
Orycterocetus crocodilinus
Tasmacetus shepherdi
Ziphius cavirostris
Mesoplodon spp.
Berardius spp.
Kentriodon pernix
Lipotes vexillifer
Platanista gangetica
Parapontoporia wilsoni
Parapontoporia sternbergi
Pontoporia blainvillei
Brachydelphis mazeasi
Pliopontos littoralis
Protophocoena minima
Stenasodelphis russellae
Auroracetus bakerae
Meherrinia isoni
Ischyrorhynchus vanbenedeni
Inia geoffrensis
Atocetus nasalis
Albireo whistleri
Monodontidae
Phocoena phocoena
Phocoenoides dalli
Leucopleurus acutus
Delphinus spp.
Tursiops truncatus
Pseudorca crassidens
Orcaella brevirostris
Orcinus orca
Globicephala spp.
Grampus griseus
2/-
2/81
4/99
>4/100
5/75
5/79
4/-
4/55
2/61
Ziphiidae +
Physeteroidea
2/58
>4/90
2/-
2/-
2/-
2/58
2/-
>4/74
Odontoceti
2/-
2/-
2/-
2/-
1/79
2/-
2/-
Inioidea
2/-
1/-
1/-
Delphinida
2/-
Pan-Iniidae
1/-
2/-
1/-
2/-
2/-
5/88
Delphinoidea
2/-
4/52
4/75
2/-
2/-
2/-
2/-
5/86

11

Figure 11

Figure 11. Life reconstruction of [redacted] by J. Molnar, feeding on a flatfish, which would have been abundant in the neritic zone of the late Miocene equatorial seas of Panama.

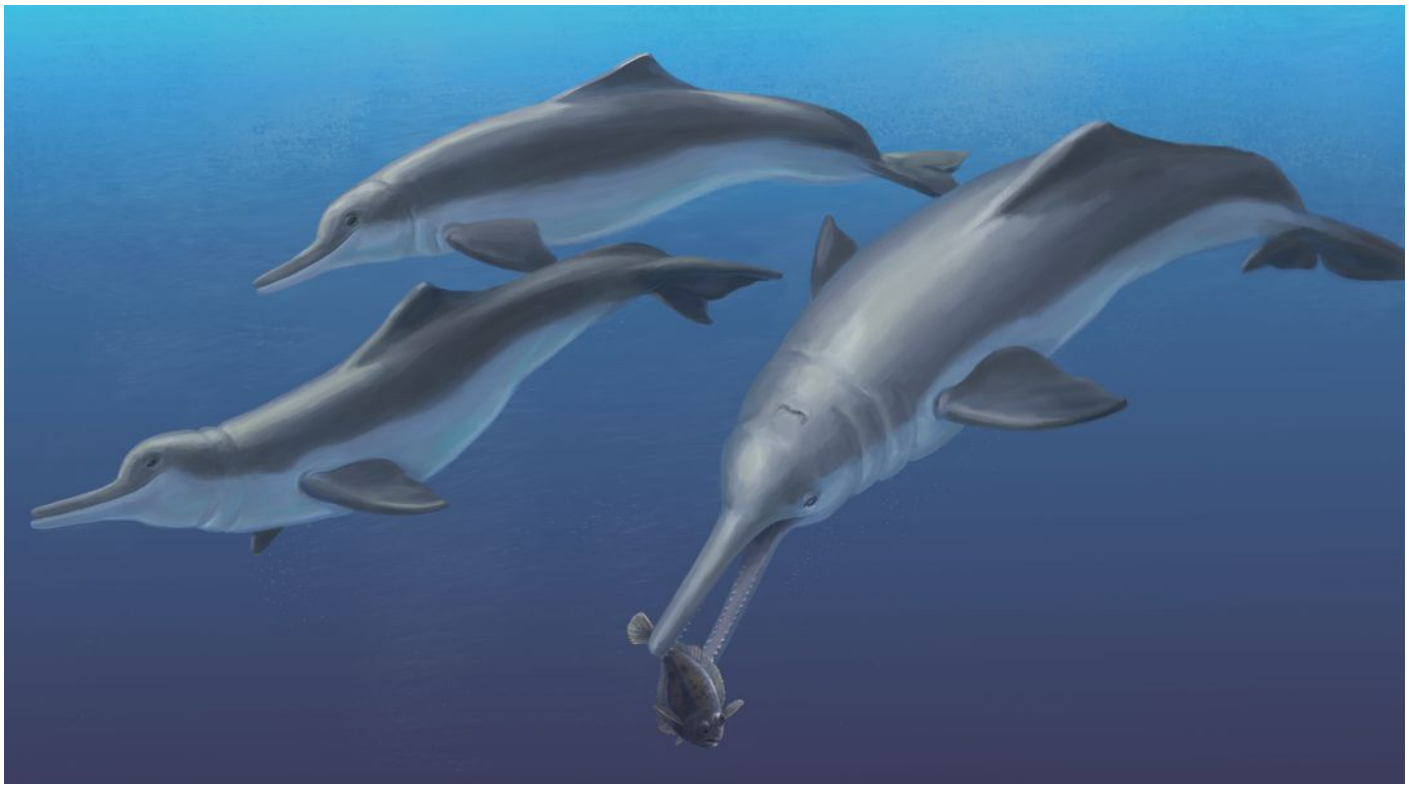

12

Figure 12

Figure 12. Time calibrated phylogenetic tree of select Delphinida, including [redacted] with Delphinoidea collapsed. Stratigraphic range data derives from published accounts for each taxon, including global ranges. Geologic time scale based on Cohen et al. (2013). Calibration for nodes follow mean divergence date estimates by McGowen et al. (2009:table 3) for the following clades: a, Delphinida (24.75 Ma); b, Inioidea+Lipotes (22.15 Ma); c, Delphinoidea (18.66 Ma); and Inioidea (in open white circle, 16.68 Ma). Arc indicates stem-based clade, Pan-Iniidae. Ecological habitat preference is based on depositional environment or extant habitat. Abbreviations: Aquitan., Aquitanian; H., Holocene; Langh., Langhian; Ma, millions of years ago; Mess., Messinian; P., Piacenzian; Ple., Pleistocene; Plioc., Pliocene; Serra., Serravallian; Zan., Zanclean.

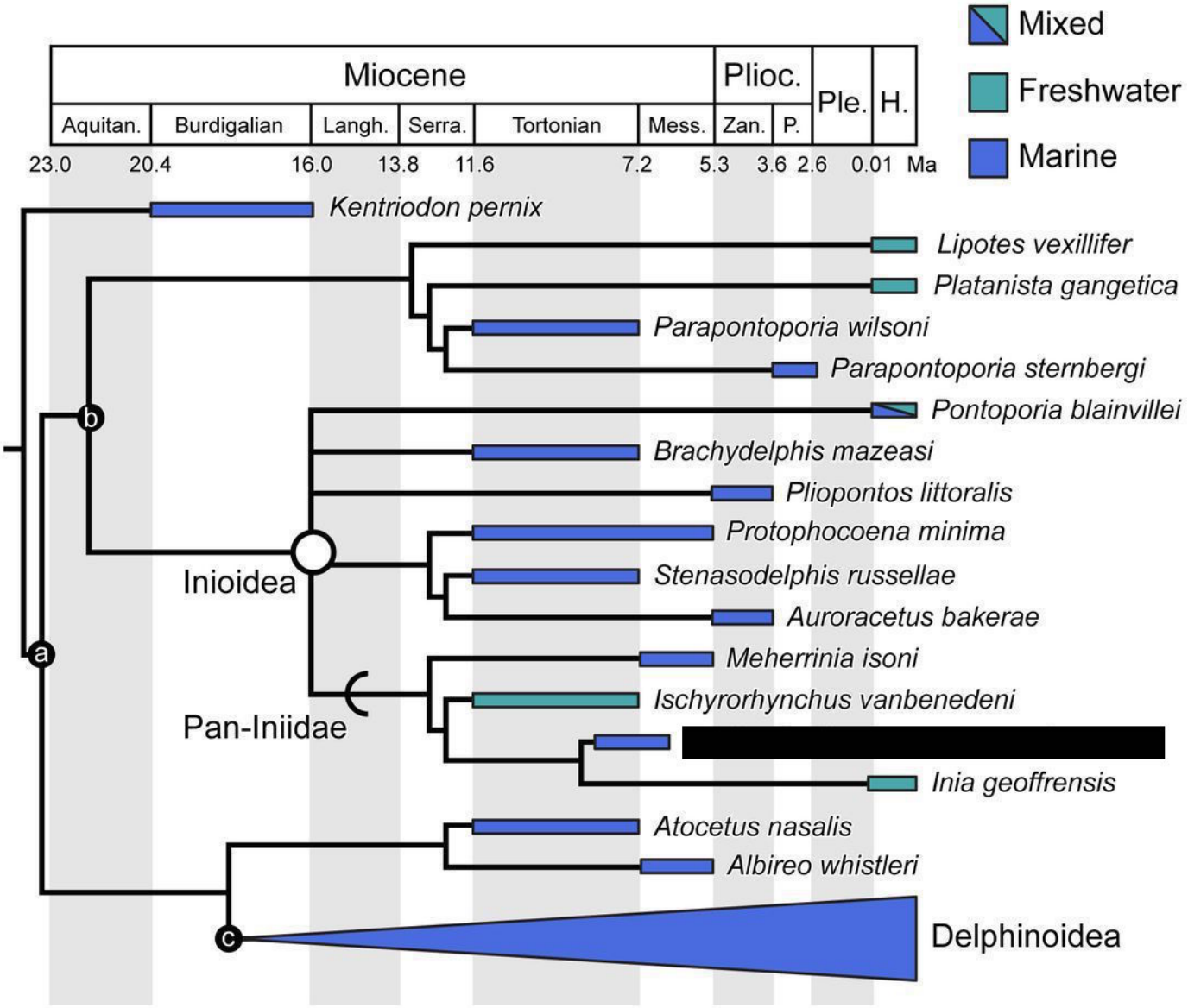
Mixed
Freshwater
Marine
Miocene
Plioc.
Ple.
H.
Aquitan.
Burdigalian
Langh.
Serra.
Tortonian
Mess.
Zan.
P.
23.0
20.4
16.0
13.8
11.6
7.2
5.3
3.6
2.6
0.01
Ma
Kentriodon pernix
Lipotes vexillifer
Platanista gangetica
Parapontoporia wilsoni
Parapontoporia sternbergi
Pontoporia blainvillei
Brachydelphis mazeasi
Pliopontos littoralis
Protophocoena minima
Stenasodelphis russellae
Auroracetus bakerae
Meherrinia isoni
Ischyrorhynchus vanbenedeni
Inia geoffrensis
Atocetus nasalis
Albireo whistleri
Delphinoidea
Inioidea
Pan-Iniidae
a
b
c